

An admissibility and asymptotic-preserving scheme for systems of conservation laws with source term on 2D unstructured meshes

F. Blachère^{a,*}, R. Turpault^b

^a *Université de Nantes, Laboratoire de Mathématiques Jean Leray, 2 rue de la Houssinière
44322 Nantes Cedex 3, France.*

^b *Bordeaux-INP, Institut de Mathématiques de Bordeaux, 351 cours de la Libération Bât
A33 33405 Talence Cedex, France.*

Abstract

The objective of this work is to design explicit finite volumes schemes for specific systems of conservation laws with stiff source terms, which degenerate into diffusion equations. We propose a general framework to design an asymptotic preserving scheme, that is stable and consistent under a classical hyperbolic CFL condition in both hyperbolic and diffusive regime, for any two-dimensional unstructured mesh. Moreover, the scheme developed also preserves the set of admissible states, which is mandatory to keep physical solutions in stiff configurations. This construction is achieved by using a non-linear scheme as a target scheme for the diffusive equation, which gives the form of the global scheme for the complete system of conservation laws. Numerical results are provided to validate the scheme in both regimes.

Keywords: finite volume schemes, 2D unstructured mesh, asymptotic-preserving schemes, admissibility-preserving schemes, conservation laws with source terms

1. Introduction

General context. The aim of this work is to design a numerical scheme to find approximate solutions to hyperbolic systems of conservation laws with source term on 2D unstructured meshes, which enter in the following formalism:

$$\partial_t \mathbf{U} + \operatorname{div}(\mathbf{F}(\mathbf{U})) = \gamma(\mathbf{U})(\mathbf{R}(\mathbf{U}) - \mathbf{U}), \quad (1.1)$$

where $\mathbf{U} \in \mathcal{A} \subset \mathbb{R}^N$, \mathcal{A} is the set of admissible states and $\mathbf{F} : \mathcal{A} \rightarrow \mathbb{R}^N$ is a smooth function whose Jacobian has real eigenvalues. The right hand side is

*Corresponding author

Email addresses: florian.blachere@univ-nantes.fr (F. Blachère),
rodolphe.turpault@u-bordeaux.fr (R. Turpault)

constituted with $\gamma : \mathcal{A} \rightarrow \mathbb{R}^+$ a positive function and $\mathbf{R} : \mathcal{A} \rightarrow \mathcal{A}$ a smooth function which fulfills the compatibility conditions stated in [5].

When $\gamma = 0$, (1.1) is nothing but the following homogeneous hyperbolic system:

$$\partial_t \mathbf{U} + \operatorname{div}(\mathbf{F}(\mathbf{U})) = 0. \quad (1.2)$$

On the other hand, due to the compatibility conditions, when $\gamma(\mathbf{U})t \rightarrow \infty$ (1.1) degenerates into a smaller diffusion system:

$$\partial_t \mathbf{u} - \operatorname{div}(\mathbf{D}(\mathbf{u})\nabla \mathbf{u}) = 0, \quad (1.3)$$

where $\mathbf{u} \in \mathcal{A}_D \subset \mathbb{R}^n$ is linked to \mathbf{U} , \mathcal{A}_D is the set of admissible states for the diffusion system and \mathbf{D} is a positive function or a symmetric, positive and definite matrix. In the framework of this work, we only focus on a degeneracy towards a diffusion equation:

$$\partial_t u - \operatorname{div}(\mathbf{D}(u)\nabla u) = 0, \quad (1.4)$$

where $u \in \mathcal{A}_D \subset \mathbb{R}$.

The two main goals are:

1. to numerically follow this degeneracy, schemes that has this behaviour are called ‘‘asymptotic-preserving’’ (AP for short) in the sense of Jin [30] (see Figure 1),
2. to preserve the set of admissible states \mathcal{A} in any regime.

Each property can be conserved separately using existing techniques but the essential difficulty is to preserve both at the same time on any unstructured mesh.

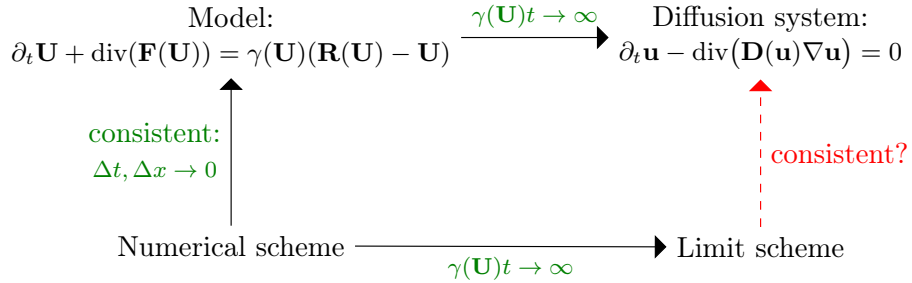


Figure 1: Aim of an AP scheme

Examples. In the set of systems that can be written as (1.1) two examples are used throughout this paper as an illustration:

(I) the isentropic Euler model with friction:

$$\mathbf{U} = \begin{pmatrix} \rho \\ \rho u \\ \rho v \end{pmatrix}, \mathbf{F}(\mathbf{U}) = \begin{pmatrix} \rho u & \rho v \\ \rho u^2 + p & \rho uv \\ \rho uv & \rho v^2 + p \end{pmatrix}, \mathbf{R}(\mathbf{U}) = \begin{pmatrix} \rho \\ 0 \\ 0 \end{pmatrix}, \quad (1.5)$$

where $\gamma(\mathbf{U}) = \kappa(\rho) > 0$ is the friction coefficient and $p(\rho)$ the pressure with $p'(\rho) > 0$.

For this model the set of admissible states is:

$$\mathcal{A} = \{\mathbf{U} = (\rho, \rho u, \rho v)^T \in \mathbb{R}^3 / \rho > 0\}. \quad (1.6)$$

When $\kappa t \rightarrow \infty$, the system degenerates into (see [28, 35] for a rigorous proof):

$$\partial_t \rho - \operatorname{div} \left(\frac{1}{\kappa(\rho)} \nabla p \right) = 0. \quad (1.7)$$

(II) the M_1 for radiative transfer [21], which may be written to enter the framework of this paper (see [7] for the reformulation):

$$\mathbf{U} = \begin{pmatrix} E \\ \mathbf{F}_R \\ T \end{pmatrix}, \mathbf{F}(\mathbf{U}) = \begin{pmatrix} \mathbf{F}_R^T \\ c^2 \mathbf{P} \\ 0 \end{pmatrix}, \mathbf{R}(\mathbf{U}) = \begin{pmatrix} \frac{\sigma^e a T^4 + \sigma_1 E}{\sigma^m} \\ \frac{\sigma_2 \mathbf{F}_R}{\sigma^m} \\ \frac{\sigma^a E}{\rho C_v \sigma^m} + \frac{\sigma_3 T}{\sigma^m} \end{pmatrix}, \quad (1.8)$$

and $\gamma(\mathbf{U}) = c\sigma_m(\mathbf{U})$. The radiative flux is defined as $\mathbf{F}_R = (F_R^x, F_R^y)^T$, and the radiative pressure is:

$$\mathbf{P} = \begin{cases} E \left(\frac{1-\chi}{2} \mathbf{I}_2 + \frac{3\chi-1}{2} \frac{\mathbf{F}_R \otimes \mathbf{F}_R}{\|\mathbf{F}_R\|} \right) & \text{if } \|\mathbf{F}_R\| \neq 0, \\ \frac{E}{3} \mathbf{I}_2 & \text{otherwise,} \end{cases}$$

where the Eddington factor is $\chi(f) = \frac{3+4f^2}{5+2\sqrt{4-3f^2}}$ and the anisotropy factor $f = \frac{\|\mathbf{F}_R\|}{cE}$.

The different $\sigma = \sigma(E, \mathbf{F}_R, T)$ are the so-called opacities, ρ is the density, C_v the volumetric heat capacity and $a \approx 7.56 \times 10^{-16}$ is the radiation constant.

The set of admissible states is:

$$\mathcal{A} = \{\mathbf{U} = (E, F_x, F_y, T)^T \in \mathbb{R}^4 / E > 0, T > 0, f \leq 1\} \quad (1.9)$$

When $c\sigma^m t \rightarrow \infty$, the system degenerates into the *equilibrium diffusion equation* [7, 36, 38]:

$$\partial_t (\rho C_v T + aT^4) - \operatorname{div} \left(\frac{c}{3\sigma^f} \nabla (aT^4) \right) = 0. \quad (1.10)$$

State of the art. The design of AP schemes in the context of hyperbolic to parabolic degeneracy is a topic of interest for more than a decade. In 1D, several AP schemes were proposed from the pioneer of Gosse and Toscani [26], where a control of the numerical diffusion is used to design an AP scheme for the Telegraph equations (also named Goldstein-Taylor equations). This technique has been extended to the M_1 for radiative transfer [12, 11, 2] and the isentropic Euler equations with friction [16]. Next, this control of the diffusion has been generalised to any system of conservation laws in 1D with the formalism (1.1) in [7, 5]. Others approaches employ the ideas of the hydrostatic reconstruction used in ‘well-balanced’ schemes to obtain AP properties for the Euler equations with friction [9] or make use of the convergence speed with finite differences schemes [1] to preserve the asymptotic behaviour.

While 2D extensions on Cartesian grids and admissible meshes (see Definition 1.1) is straightforward as the schemes can be easily reformulated as convex combination of 1D schemes that have the AP property [6, 40], the problem is much more difficult on unstructured meshes since most schemes degenerate into the TP scheme (a.k.a FV4 [23]), which is not consistent on unstructured meshes. Two main approaches exist to obtain AP schemes on unstructured grids: the first one is an MPFA based scheme essentially developed for Friedrichs systems in [13, 14, 25], which degenerates into the scheme developed in [10], and the preservation of \mathcal{A} is not guaranteed with the explicit version of this scheme. The second one is the scheme developed in [6] which is based on the diamond scheme [18] and the technique developed in [7] which leads to a correct discretization of the diffusion limit, but the preservation of \mathcal{A} is only satisfied under a geometrical condition on the mesh. The same kind of technique has been use on the shallow water equations with Manning-type friction in [22], but the preservation of \mathcal{A} is only proved by numerical tests.

Aim. The objective of this work is to design an explicit finite volume scheme which is AP and preserves \mathcal{A} under a classical CFL condition. This will allow extensions to a high-order schemes which preserve \mathcal{A} under a CFL directly linked to the explicit first order one (let us also recall that the second Dahlquist barrier [19] forbids unconditionally stable implicit schemes of order greater than two). This scheme will preserve the set of admissible states \mathcal{A} and the asymptotic behaviour on any 2D unstructured meshes. Moreover, it will be flexible in the sense that it can be applied to any hyperbolic system of conservation laws (1.1), and the extension of any consistent 1D two-points approximate Riemann solver may be obtained.

Outline. The first part of this paper is dedicated to the development of the scheme for the hyperbolic system (1.2), obviously by bearing in mind the AP property that will be needed with the introduction of the source term. A theorem is presented in order to guarantee the preservation of the set of admissible states \mathcal{A} under a classical CFL condition for hyperbolic systems. The scheme is constructed in the spirit of the one developed by Droniou and Le Potier [20] (DLP for short), which will be a relevant limit scheme for the discretization of

the limit equation (1.4). Finally, a procedure allows the new scheme to correctly enter the framework of the theorem.

Then, the second part is devoted to extend the previous scheme, in order to take into account the source term of (1.1), using the technique developed in [7]. An additional result proves that it is possible to obtain an AP scheme that degenerates into the DLP scheme and preserves the set of admissible states \mathcal{A} under the same CFL condition used for the homogeneous system (1.1).

In both cases, numerical examples illustrate the behaviour of the scheme.

Mesh notations. For this work the following classical notations are used to describe the mesh (see Figure 2):

- \mathcal{M} is an unstructured mesh constituted of polygonal cells K ,
- \mathbf{x}_K is the center of the cell K ,
- L is the neighbor of K by the interface i , $i = K \cap L$,
- $KL = \overrightarrow{\mathbf{x}_K \mathbf{x}_L}$,
- \mathcal{E}_K is the set of the interfaces of K ,
- $|e_i|$ is length of the interface i ,
- $|K|$ is the area of the cell K .

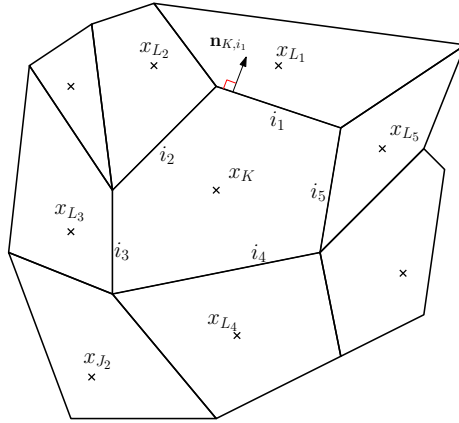


Figure 2: Notations for unstructured mesh

In the framework of unstructured meshes, it is often convenient to consider the so-called admissible meshes:

Definition 1.1. *An interface i is said to be admissible if and only if:*

$$KL \cdot \mathbf{n}_{K,i} = \|KL\|.$$

A mesh is said to be admissible if and only if all its interfaces are admissible. Cartesian grids or triangular meshes with cell center located at the center of the circumscribed circle (Delaunay triangulation) are therefore admissible for instance.

2. Numerical scheme for hyperbolic system

2.1. Main results

In this section, a numerical scheme is designed for the hyperbolic system (1.2). This scheme will be extended to take into account the source term in the next section.

The construction of this scheme focuses on the following points:

- (i) the numerical diffusion occurs in the direction $\mathbf{n}_{K,i}$,
- (ii) the flux used in the scheme is an extension of a 1D two-points approximate Riemann solver,
- (iii) the set of admissible states \mathcal{A} has to be conserved under a suitable CFL condition.

The point (i) will be necessary to include the source term in the next section and (ii) provides a general framework. Finally, the point (iii) is one of the main objectives of the development.

Besides, the construction is focused on explicit Euler schemes for the time discretization, since a CFL condition for this case allows considering very high order extension (cf. SSPRK schemes [27]). For the sake of clarity, the time dependency of every term is omitted except when it is necessary, since only the explicit Euler scheme is used.

In this context, we propose to consider a conservative explicit finite volume scheme which may therefore be given by the following expression:

$$\forall K \in \mathcal{M}, \mathbf{U}_K^{n+1} = \mathbf{U}_K^n - \frac{\Delta t}{|K|} \sum_{i \in \mathcal{E}_K} |e_i| \mathcal{F}_i \cdot \mathbf{n}_{K,i}, \quad (2.1)$$

where the numerical flux approximates the physical flux: $\mathcal{F}_i \cdot \mathbf{n}_{K,i} \simeq \mathbf{F}(\mathbf{U}_K^n) \cdot \mathbf{n}_{K,i}|_{e_i, t=t^n}$.

Let us first give a result that provides a general framework to design a scheme adapted to our problem. We focus on specific choices of \mathcal{F}_i to preserve the set of admissible states \mathcal{A} as stated in the following theorem:

Theorem 2.1. *We assume that the conservative numerical flux \mathcal{F}_i has the following properties:*

1. *Consistency:*
if $\forall K \in \mathcal{M}, \mathbf{U}_K^n = \mathbf{U}$ then $\forall K \in \mathcal{M}, \forall i \in \mathcal{E}_K, \mathcal{F}_i \cdot \mathbf{n}_{K,i} = \mathbf{F}(\mathbf{U}) \cdot \mathbf{n}_{K,i}$,
2. *Admissibility:*

(a) $\forall K \in \mathcal{M}, \forall i \in \mathcal{E}_K, \forall J \in \mathcal{S}_{K,i}, \exists \nu_{K,i}^J \geq 0$ such that:

$$\mathcal{F}_i \cdot \mathbf{n}_{K,i} = \sum_{J \in \mathcal{S}_{K,i}} \nu_{K,i}^J \mathcal{F}_{KJ} \cdot \boldsymbol{\eta}_{KJ},$$

with $\mathcal{F}_{KJ} \cdot \boldsymbol{\eta}_{KJ} = \mathcal{F}(\mathbf{U}_K, \mathbf{U}_J; \boldsymbol{\eta}_{KJ})$ a consistent two-points approximate Riemann solver,

(b) for any constant vector \mathbf{V} , $\forall K \in \mathcal{M}, \sum_{i \in \mathcal{E}_K} |e_i| \sum_{J \in \mathcal{S}_{K,i}} \nu_{K,i}^J \mathbf{V} \cdot \boldsymbol{\eta}_{KJ} = 0$,

with $\mathcal{S}_{K,i}$ the set of points used to reconstruct the flux on the interface i and $\boldsymbol{\eta}_{KJ}$ is a unitary vector outgoing of K .

Then the scheme (2.1) is stable, and preserves the space of admissible states \mathcal{A} as soon as the following classical CFL condition is fulfilled:

$$\max_{\substack{K \in \mathcal{M} \\ J \in \bar{\mathcal{E}}_K}} \left(b_{KJ} \frac{\Delta t}{\delta_{KJ}} \right) \leq 1, \quad (2.2)$$

where b_{KJ} is the greatest speed of the numerical flux between the states \mathbf{U}_K^n and \mathbf{U}_J^n , and δ_{KJ} is a characteristic length that is defined later (see (2.5)).

Moreover, if \mathcal{F}_{KJ} is the flux of an entropic 1D scheme, then the scheme (2.1) is entropic.

Proof. The outline of the proof is to write the scheme as a convex combination of 1D schemes as it was done for instance in [37, 6]. Obviously, the aim is to obtain 1D schemes which fulfill the expected properties.

With the property 2a the scheme (2.1) can be expressed as:

$$\mathbf{U}_K^{n+1} = \mathbf{U}_K^n - \frac{\Delta t}{|K|} \sum_{i \in \mathcal{E}_K} |e_i| \mathcal{F}_i^n \cdot \mathbf{n}_{K,i} \quad (2.1)$$

$$= \mathbf{U}_K^n - \frac{\Delta t}{|K|} \sum_{i \in \mathcal{E}_K} |e_i| \sum_{J \in \mathcal{S}_{K,i}} \nu_{K,i}^J \mathcal{F}_{KJ} \cdot \boldsymbol{\eta}_{KJ}. \quad (2.3)$$

The inversion of the two sums gives:

$$\mathbf{U}_K^{n+1} = \mathbf{U}_K^n - \frac{\Delta t}{|K|} \sum_{J \in \bar{\mathcal{E}}_K} \left(\sum_{i \in \bar{\mathcal{S}}_{KJ}} |e_i| \nu_{K,i}^J \right) \mathcal{F}_{KJ} \cdot \boldsymbol{\eta}_{KJ}, \quad (2.4)$$

where:

- $\bar{\mathcal{E}}_K = \cup_{i \in \mathcal{E}_K} \mathcal{S}_{K,i}$ is the set of points used to reconstruct all the fluxes on the cell K (stencil of the cell K),
- $\bar{\mathcal{S}}_{KJ} = \{i/J \in \mathcal{S}_{K,i}\}$ are the indexes of the interfaces of K which used the value of the solution on \boldsymbol{x}_J (\mathbf{U}_J^n) to reconstruct the flux on the interface i . See for instance Figure 5 for more details about these spaces.

The length $d_{KJ} := \sum_{i \in \mathcal{S}_{K,i}} |e_i| \nu_{K,i}^J > 0$, is introduced to turn (2.4) into:

$$\mathbf{U}_K^{n+1} = \mathbf{U}_K^n - \frac{\Delta t}{|K|} \sum_{J \in \bar{\mathcal{E}}_K} d_{KJ} \mathcal{F}_{KJ} \cdot \boldsymbol{\eta}_{KJ}.$$

In order to rewrite this expression as a convex combination of 1D schemes, a positive coefficient $\omega_{KJ} := \frac{d_{KJ}}{\sum_{J \in \bar{\mathcal{E}}_K} d_{KJ}}$ is used to obtain:

$$\mathbf{U}_K^{n+1} = \sum_{J \in \bar{\mathcal{E}}_K} \omega_{KJ} \mathbf{U}_K^{n+1} = \sum_{J \in \bar{\mathcal{E}}_K} \left(\omega_{KJ} \mathbf{U}_K^n - \frac{\Delta t}{|K|} d_{KJ} \mathcal{F}_{KJ} \cdot \boldsymbol{\eta}_{KJ} \right),$$

since $\sum_{J \in \bar{\mathcal{E}}_K} \omega_{KJ} = 1$.

This expression may be simplified by setting:

$$\delta_{KJ} := \frac{|K|}{\sum_{J \in \bar{\mathcal{E}}_K} d_{KJ}} > 0, \quad (2.5)$$

which can be assimilated to a space step, to have:

$$\sum_{J \in \bar{\mathcal{E}}_K} \omega_{KJ} \mathbf{U}_K^{n+1} = \sum_{J \in \bar{\mathcal{E}}_K} \omega_{KJ} \left(\mathbf{U}_K^n - \frac{\Delta t}{\delta_{KJ}} \mathcal{F}_{KJ} \cdot \boldsymbol{\eta}_{KJ} \right). \quad (2.6)$$

Now, to obtain a convex combination of 1D schemes, a term has to be introduced to play the role of the flux on the left interface.

With the newly introduced coefficients the assumption 2b in the Theorem 2.1 could be reformulated into a discrete divergence formula:

$$\sum_{i \in \mathcal{E}_K} |e_i| \sum_{J \in \mathcal{S}_{K,i}} \nu_{K,i}^J \boldsymbol{\eta}_{KJ} = 0 \iff \sum_{J \in \bar{\mathcal{E}}_K} d_{KJ} \boldsymbol{\eta}_{KJ} = 0. \quad (2.7)$$

This condition is fulfilled when the ‘virtual cells’ are closed. The ‘virtual cells’ may be seen as polygonal cells where the interfaces are orthogonal to $\boldsymbol{\eta}_{KJ}$ with a length of d_{KJ} . This reformulation leads to:

$$\frac{\Delta t}{|K|} \mathbf{F}(\mathbf{U}_K^n) \cdot \sum_{J \in \bar{\mathcal{E}}_K} d_{KJ} \boldsymbol{\eta}_{KJ} = 0.$$

And then by using the previously defined coefficients:

$$\begin{aligned} \sum_{J \in \bar{\mathcal{E}}_K} d_{KJ} \frac{\Delta t}{|K|} \mathbf{F}(\mathbf{U}_K^n) \cdot \boldsymbol{\eta}_{KJ} &= \sum_{J \in \bar{\mathcal{E}}_K} \omega_{KJ} \frac{\Delta t}{\delta_{KJ}} \mathbf{F}(\mathbf{U}_K^n) \cdot \boldsymbol{\eta}_{KJ} \\ &= \sum_{J \in \bar{\mathcal{E}}_K} \omega_{KJ} \frac{\Delta t}{\delta_{KJ}} \mathcal{F}_{KJ} \cdot \boldsymbol{\eta}_{KJ} = 0, \end{aligned} \quad (2.8)$$

we defined $\mathcal{F}_{KJ} := \mathbf{F}(\mathbf{U}_K^n)$ as the two-points approximate Riemann solver \mathcal{F} is consistent.

Then, the term of (2.8) can be added in the previous convex combination of schemes (2.6):

$$\sum_{J \in \bar{\mathcal{E}}_K} \omega_{KJ} \mathbf{U}_K^{n+1} = \sum_{J \in \bar{\mathcal{E}}_K} \omega_{KJ} \left(\mathbf{U}_K^n - \frac{\Delta t}{\delta_{KJ}} [\mathcal{F}_{KJ} - \mathcal{F}_{KK}] \cdot \boldsymbol{\eta}_{KJ} \right). \quad (2.9)$$

Finally, the scheme (2.9) is rewritten as a convex combination of 1D schemes in the direction KJ with \mathbf{U}_K as a left state, \mathbf{U}_J on the right and \mathbf{U}_K also in intermediary state (see Figure 3).



Figure 3: States between cells for 1D and 2D schemes

As such, this scheme is stable and preserves the set of admissible states \mathcal{A} under the classical 1D CFL condition linked to the flux \mathcal{F}_{KJ} :

$$\max_{\substack{K \in \mathcal{M} \\ J \in \bar{\mathcal{E}}_K}} \left(b_{KJ} \frac{\Delta t}{\delta_{KJ}} \right) \leq 1, \quad (2.2)$$

where b_{KJ} is the greatest speed of the numerical flux \mathcal{F}_{KJ} between the states \mathbf{U}_K^n and \mathbf{U}_J^n . This CFL condition is majored by 1 as the state \mathbf{U}_K is involved twice in the Riemann problem.

In addition, the scheme is also entropic as soon as \mathcal{F}_{KJ} is the flux of a 1D entropic scheme. \square

Remark 2.1. *Let us notice that the proof of this theorem can be straightforwardly extended to replace the explicit Euler scheme in (2.1) by any Runge-Kutta time integration. In that case, the CFL condition (2.2) is modified accordingly. For instance, an implicit Euler version of the scheme may be designed and will be unconditionally stable. Let us also point out that the ν coefficients involved in property 2a may depend on the solution. In that case, the computational cost of implicit schemes quickly becomes important.*

2.2. A possible choice of flux

A possible choice for \mathcal{F}_i is the classical two-points (TP) flux, for instance with the Rusanov approximation [39]:

$$\mathcal{F}_i \cdot \mathbf{n}_{K,i} = \frac{\mathbf{F}(\mathbf{U}_K^n) + \mathbf{F}(\mathbf{U}_L^n)}{2} \cdot \mathbf{n}_{K,i} - \frac{b_{KL}}{2} (\mathbf{U}_L^n - \mathbf{U}_K^n). \quad (2.10)$$

This flux is consistent, conservative and fulfills the conditions of the theorem with $\mathcal{S}_{K,i} = L$, $\boldsymbol{\eta}_{KL} = \mathbf{n}_{K,i}$ and $\nu_{K,i}^L = 1$. Moreover, the condition 2b is verified with any polygonal cells, as a consequence of the divergence formula. Therefore,

a scheme based on the flux (2.10) is stable and preserves the set of admissible states \mathcal{A} under the CFL condition given by (2.2).

However, this choice does not allow us to design an AP scheme since the numerical diffusion occurs in the direction KL instead of $\mathbf{n}_{K,i}$, as stated in the point (i). In fact, this choice of \mathcal{F}_i leads to the FV4 scheme [23] in the diffusion limit, nevertheless, this limit scheme is not consistent with the diffusion equation unless the mesh is admissible (see for instance [40, 6] for a proof).

Hence, we will consider schemes with a numerical diffusion in the direction $\mathbf{n}_{K,i}$.

2.3. A better choice of flux: the HLL-DLP flux

To have a relevant discretization of the gradient in the asymptotic limit and have AP properties, we propose to design a scheme in the spirit of the one developed by Droniou and Le Potier [20], in order to target the DLP scheme in the diffusive limit and have the numerical diffusion oriented through the normal $\mathbf{n}_{K,i}$ (i).

Their scheme is non-linear and preserves the set of admissible states for elliptic equations. In this framework this preservation is difficult, indeed, few schemes for the Laplace equation preserve the set of admissible states. Let us mention some of them: the diamond scheme [18] on particular meshes (see [6]), the non-linear correction introduced by Le Potier in [32] and extended in [15, 33] applied on any consistent and conservative schemes and the DLP scheme.

The DLP scheme was selected, as the expression of the discrete gradient is well suited for our applications, hence, the normal discrete gradient with the DLP scheme can be expressed as:

$$\nabla u_K \cdot \mathbf{n}_{K,i} = \sum_{J \in \mathcal{S}_{K,i}} \bar{\nu}_{K,i}^J(u)(u_J - u_K), \quad (2.11)$$

with $\bar{\nu}_{K,i}^J \geq 0$, this positivity enforces the preservation of \mathcal{A}_D and is a significant feature to incorporate into our scheme for hyperbolic systems (2.1).

Using the same notations as in their work, the numerical flux \mathcal{F}_i is built in the same fashion as their flux for elliptic equations but obviously adapted to hyperbolic problems, and will be named HLL-DLP flux. The values of the $\nu_{K,i}^J$ coefficients used in Theorem 2.1 are exhibited by the following computations.

2.3.1. Interpolation

First, two points M are introduced per interface i (see Figure 4):

- $\mathbf{x}_{M_{K,i}}$ belongs to the half line of direction $\mathbf{n}_{K,i}$ starting at \mathbf{x}_K ,
- $\mathbf{x}_{M_{L,i}}$ belongs to the half line of direction $\mathbf{n}_{L,i} = -\mathbf{n}_{K,i}$ starting at \mathbf{x}_L .

Let us note that these half lines do not necessarily cross the interface i .

These points $\mathbf{x}_{M_{K,i}}$ and $\mathbf{x}_{M_{L,i}}$ can be defined as a convex combination of cell centers in \mathcal{M} as in [20] (the same thing is done with the diamond scheme [18])

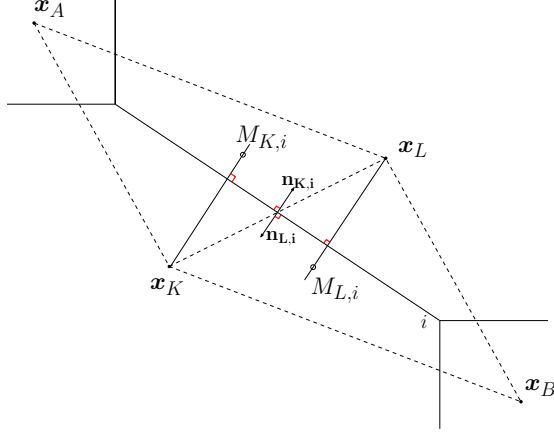


Figure 4: Definition of the points M .

for the interpolation of the values at the vertices):

$$\begin{cases} \mathbf{x}_{M_{K,i}} &= \sum_{J \in \mathcal{S}_{K,i}} w_{K,i}^J \mathbf{x}_J \\ \mathbf{x}_{M_{L,i}} &= \sum_{J \in \mathcal{S}_{L,i}} w_{L,i}^J \mathbf{x}_J, \end{cases} \quad (2.12)$$

where $w_{K,i}^J, w_{L,i}^J \geq 0$, and $\sum_{J \in \mathcal{S}_{K,i}} w_{K,i}^J = \sum_{J \in \mathcal{S}_{L,i}} w_{L,i}^J = 1$. The value of the solution at these points is interpolated using the same construction (2.12).

The definitions of $\mathbf{x}_{M_{K,i}}$ and $\mathbf{x}_{M_{L,i}}$ implies that:

$$\begin{cases} KM_{K,i} &= \sum_{J \in \mathcal{S}_{K,i}} w_{K,i}^J KJ, \\ LM_{L,i} &= \sum_{J \in \mathcal{S}_{L,i}} w_{L,i}^J LJ, \end{cases} \quad (2.13)$$

and the reconstruction of the outward normals in each cell is given by:

$$\left\{ \begin{array}{l} \mathbf{n}_{K,i} = \frac{KM_{K,i}}{\|KM_{K,i}\|} = \sum_{J \in \mathcal{S}_{K,i}} \frac{w_{K,i}^J}{\|KM_{K,i}\|} KJ = \sum_{J \in \mathcal{S}_{K,i}} \frac{w_{K,i}^J \|KJ\|}{\|KM_{K,i}\|} \boldsymbol{\eta}_{KJ} \\ \hspace{15em} = \sum_{J \in \mathcal{S}_{K,i}} \bar{w}_{K,i}^J \boldsymbol{\eta}_{KJ}, \\ \mathbf{n}_{L,i} = \frac{LM_{L,i}}{\|LM_{L,i}\|} = \sum_{J \in \mathcal{S}_{L,i}} \frac{w_{L,i}^J}{\|LM_{L,i}\|} LJ = \sum_{J \in \mathcal{S}_{L,i}} \frac{w_{L,i}^J \|LJ\|}{\|LM_{L,i}\|} \boldsymbol{\eta}_{LJ} \\ \hspace{15em} = \sum_{J \in \mathcal{S}_{L,i}} \bar{w}_{L,i}^J \boldsymbol{\eta}_{LJ}, \end{array} \right. \quad (2.14)$$

where $\mathbf{n}_{K,i} = -\mathbf{n}_{L,i}$ and $\boldsymbol{\eta}_{KJ} = \frac{KJ}{\|KJ\|}$ is the unit vector in the direction of KJ .

Remark 2.2.

- The point \mathbf{x}_L has to be in $\mathcal{S}_{K,i}$ but it is not mandatory for \mathbf{x}_K , as it will be show in the construction of the flux \mathcal{F}_i .

- For the sake of accuracy, the points chose to reconstruct the two points M should be as close of \mathbf{x}_K and \mathbf{x}_L as possible.

Equipped with these definitions, the set of points defined in the theorem and used in the proof are the following:

- $\mathcal{S}_{K,i}$ are the points used to reconstruct $\mathbf{x}_{M_{K,i}}$ (not necessarily neighbors of K),
- $\bar{\mathcal{E}}_K = \cup_{i \in \mathcal{E}_K} \mathcal{S}_{K,i}$ are the points used to reconstruct all the points $\mathbf{x}_{M_{K,i}}$ (stencil of the cell K),
- $\bar{\mathcal{S}}_{KJ} = \{i/J \in \mathcal{S}_{K,i}\}$ are the indexes of the interfaces of K which use \mathbf{x}_J to reconstruct $\mathbf{x}_{M_{K,i}}$.

For the rest of the computations we will use the barycentric coordinates for the convex combinations (2.12). From the definition of the barycentric coordinates all the coefficients $w_{K,i}^J$ (resp. $w_{L,i}^J$) are positive if the points $\mathbf{x}_{M_{K,i}}$ (resp. $\mathbf{x}_{M_{L,i}}$) lie into the polygon created by the points of $\mathcal{S}_{K,i}$ (resp. $\mathcal{S}_{L,i}$). Furthermore, we have $\sum_{J \in \mathcal{S}_{K,i}} w_{K,i}^J = \sum_{J \in \mathcal{S}_{L,i}} w_{L,i}^J = 1$.

The computation of the barycentric coordinates are direct for a starred polygon in 2D. For instance, we use the mean values coordinates from [24]. Let us point out that, even if a wide variety of possibilities exists for the choice of $\mathcal{S}_{K,i}$, only sets of three points will be used for practical applications in this article.

As an example, let us give some sets constructed with three points from Figure 5:

- $\mathcal{S}_{K,i_3} = \{\mathbf{x}_{L_3}, \mathbf{x}_K, \mathbf{x}_{J_1}\}$,
- $\bar{\mathcal{E}}_K = \{\mathbf{x}_{L_1}, \mathbf{x}_{L_2}, \mathbf{x}_K, \mathbf{x}_{J_1}, \mathbf{x}_{L_3}, \mathbf{x}_{L_4}, \mathbf{x}_{J_3}, \mathbf{x}_{L_5}\}$,
- $\bar{\mathcal{S}}_{KJ_1} = \{i_2, i_3\}$.

Remark 2.3. *The numerical cost of these new quantities is neglectable compared to the cost of the global scheme. It is in the same magnitude as the computations of the geometrical elements for an unstructured mesh.*

2.3.2. Expression of the numerical fluxes

An extension of the Rusanov scheme using the DLP reconstruction is proposed in this paragraph for the sake of simplicity in the notations. Let us emphasize that the extension to other two-points approximate Riemann solvers such as HLL [29] or HLLC (see [42, 43] for Euler and [2, 4] for the M_1 model) is straightforward. The extension with the HLL scheme will be used for some numerical tests.

A Rusanov flux is hence used in each direction (for each $J \in \mathcal{S}_{K,i}$):

$$\mathcal{F}_{KJ} \cdot \boldsymbol{\eta}_{KJ} = \frac{\mathbf{F}(\mathbf{U}_J^n) + \mathbf{F}(\mathbf{U}_K^n)}{2} \cdot \boldsymbol{\eta}_{KJ} - \frac{b_{KJ}}{2} (\mathbf{U}_J^n - \mathbf{U}_K^n), \quad (2.15)$$

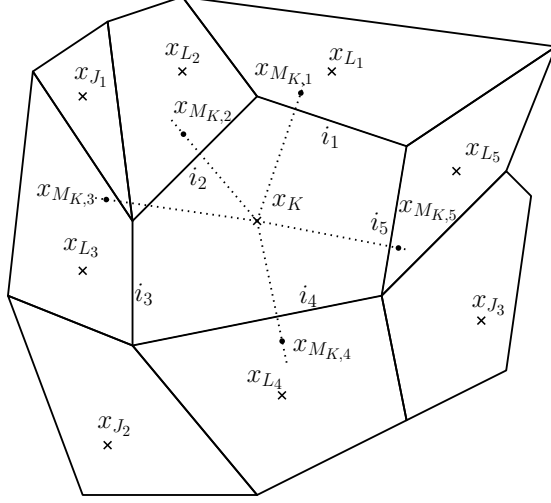


Figure 5: Representation of the set of points

where b_{KJ} is the speed of the Rusanov scheme (which is therefore larger than all wave speeds at the interface between K and J).

In order to have a consistent combination of fluxes $\mathcal{F}_{KJ} \cdot \boldsymbol{\eta}_{KJ}$ which leads to a consistent formulation of $\mathcal{F}_{K,i} \cdot \mathbf{n}_{K,i}$, the following reconstruction, from the one of the normal vector (2.14), is used:

$$\mathcal{F}_{K,i} \cdot \mathbf{n}_{K,i} = \sum_{J \in \mathcal{S}_{K,i}} \bar{w}_{K,i}^J \mathcal{F}_{KJ} \cdot \boldsymbol{\eta}_{KJ}. \quad (2.16)$$

The consistency is guaranteed by the properties coming from the barycentric coordinates: $\sum_{J \in \mathcal{S}_{L,i}} \bar{w}_{L,i}^J \boldsymbol{\eta}_{KJ} = \mathbf{n}_{K,i}$ (2.14), and the fact that \mathcal{F}_{KJ} is a consistent flux. Similarly, $\mathcal{F}_{L,i}$ is defined as:

$$\mathcal{F}_{L,i} \cdot \mathbf{n}_{L,i} = \sum_{J \in \mathcal{S}_{L,i}} \bar{w}_{L,i}^J \mathcal{F}_{LJ} \cdot \boldsymbol{\eta}_{LJ}. \quad (2.17)$$

Following the strategy of Droniou and Le Potier in [20] \mathcal{F}_i is introduced as a convex combination of $\mathcal{F}_{K,i}$ and $\mathcal{F}_{L,i}$. Hence, for each component j of the system (1.2):

$$\mathcal{F}_i^j = \gamma_{K,i}^j \mathcal{F}_{K,i}^j + \gamma_{L,i}^j \mathcal{F}_{L,i}^j, \quad (2.18)$$

where $\gamma_{L,i}^j, \gamma_{K,i}^j \geq 0$, have to be chosen such that $\gamma_{L,i}^j + \gamma_{K,i}^j = 1$.

This expression of \mathcal{F}_i^j allows us to write on the one hand:

$$\mathcal{F}_i^j \cdot \mathbf{n}_{K,i} = \gamma_{K,i}^j \mathcal{F}_{K,i}^j \cdot \mathbf{n}_{K,i} - \gamma_{L,i}^j \mathcal{F}_{L,i}^j \cdot \mathbf{n}_{L,i} \quad (2.19)$$

$$:= \sum_{J \in \mathcal{S}_{K,i}} v_{K,i}^{J,j} \mathcal{F}_{KJ} \cdot \boldsymbol{\eta}_{KJ}, \quad (2.20)$$

and on the other hand:

$$\mathcal{F}_i^j \cdot \mathbf{n}_{L,i} = -\gamma_{K,i}^j \mathcal{F}_{K,i}^j \cdot \mathbf{n}_{K,i} + \gamma_{L,i}^j \mathcal{F}_{L,i}^j \cdot \mathbf{n}_{L,i} \quad (2.21)$$

$$:= \sum_{J \in \mathcal{S}_{L,i}} \nu_{L,i}^{J,j} \mathcal{F}_{LJ}^j \cdot \boldsymbol{\eta}_{LJ}. \quad (2.22)$$

Let us emphasize that this numerical flux $\mathcal{F}_i (= (\mathcal{F}_i^j)_j)$ is consistent, conservative and non-linear by construction.

The choice of $\gamma_{K,i}^j$ and $\gamma_{L,i}^j$ now has to be made in order to enforce the positivity of the coefficients $\nu_{K,i}^{J,j}$ and $\nu_{L,i}^{J,j}$. In order to do so, the fluxes \mathcal{F}_i^j are decomposed by introducing $\beta_i := \min(\bar{w}_{K,i}^L, \bar{w}_{L,i}^K)$:

$$\begin{cases} \mathcal{F}_{K,i}^j \cdot \mathbf{n}_{K,i} &= \beta_i \mathcal{F}_{KL}^j \cdot \boldsymbol{\eta}_{KL} + G_{K,i}^j, \\ \mathcal{F}_{L,i}^j \cdot \mathbf{n}_{L,i} &= \beta_i \mathcal{F}_{LK}^j \cdot \boldsymbol{\eta}_{LK} + G_{L,i}^j. \end{cases} \quad (2.23)$$

This leads to the expression of $G_{K,i}^j$ and $G_{L,i}^j$:

$$\begin{cases} G_{K,i}^j &= (\bar{w}_{K,i}^L - \beta_i) \mathcal{F}_{KL}^j \cdot \boldsymbol{\eta}_{KL} + \sum_{J \in \{\mathcal{S}_{K,i} \setminus L\}} \bar{w}_{K,i}^J \mathcal{F}_{KJ}^j \cdot \boldsymbol{\eta}_{KJ}, \\ G_{L,i}^j &= (\bar{w}_{L,i}^K - \beta_i) \mathcal{F}_{LK}^j \cdot \boldsymbol{\eta}_{LK} + \sum_{J \in \{\mathcal{S}_{L,i} \setminus K\}} \bar{w}_{L,i}^J \mathcal{F}_{LJ}^j \cdot \boldsymbol{\eta}_{LJ}. \end{cases} \quad (2.24)$$

Now, the $\gamma_{K,i}^j$ and $\gamma_{L,i}^j$ coefficients have to be chosen in order to balance the negative coefficients. The choice made by Droniou and Le Potier is the following:

$$\begin{cases} \gamma_{K,i}^j &= \frac{|G_{L,i}^j|}{|G_{K,i}^j| + |G_{L,i}^j|} \\ \gamma_{L,i}^j &= \frac{|G_{K,i}^j|}{|G_{K,i}^j| + |G_{L,i}^j|} \end{cases} \in [0; 1]^2, \quad (2.25)$$

with $\gamma_{K,i}^j = \gamma_{L,i}^j = \frac{1}{2}$ if $|G_{K,i}^j| + |G_{L,i}^j| = 0$.

With these coefficients and after some computations, the flux may now be expressed as a combination of fluxes in the direction KJ with positive coefficients:

$$\begin{aligned} \mathcal{F}_i^j \cdot \mathbf{n}_{K,i} &= \begin{cases} \beta_i \mathcal{F}_{KL}^j \cdot \boldsymbol{\eta}_{KL} & \text{if } G_{K,i}^j G_{L,i}^j \geq 0, \\ (\beta_i + 2\gamma_{K,i}^j (\bar{w}_{K,i}^L - \beta_i)) \mathcal{F}_{KL}^j \cdot \boldsymbol{\eta}_{KL} \\ + 2\gamma_{K,i}^j \sum_{J \in \{\mathcal{S}_{K,i} \setminus L\}} \bar{w}_{K,i}^J \mathcal{F}_{KJ}^j \cdot \boldsymbol{\eta}_{KJ} & \text{otherwise,} \end{cases} \\ &:= \sum_{J \in \mathcal{S}_{K,i}} \nu_{K,i}^{J,j} \mathcal{F}_{KJ}^j \cdot \boldsymbol{\eta}_{KJ}. \end{aligned} \quad (2.26)$$

The positivity of all the ν coefficients is enforced by the choice of β_i , the properties on $\gamma_{K,i}^j$ and the positivity of the barycentric coordinates. Furthermore, the numerical flux $\mathcal{F}_i (= (\mathcal{F}_i^j)_j)$ is conservative and consistent by construction.

As previously stated it is also possible to use any two-points approximate Riemann solver for \mathcal{F}_{KJ} , since the choice of the Rusanov flux does not have

any incidence on the construction of the flux \mathcal{F}_i . Let also us remind that this flux (2.26) will be named HLL-DLP for the rest of the paper, as is it extended from an HLL flux (Rusanov) with the DLP reconstruction.

Remark 2.4.

- With these coefficients we have:

$$\sum_{J \in \mathcal{S}_{K,i}} \nu_{K,i}^{J,j} \boldsymbol{\eta}_{KJ} = \begin{cases} \beta_i \boldsymbol{\eta}_{KL} & \text{if } G_{K,i}^j G_{L,i}^j \geq 0, \\ 2\gamma_{K,i}^j \mathbf{n}_{K,i} + \beta_i (\gamma_{L,i}^j - \gamma_{K,i}^j) \boldsymbol{\eta}_{KL} & \text{otherwise.} \end{cases} \quad (2.27)$$

- For the boundary fluxes a simpler definition is used, which does not use any reconstruction:

$$\mathcal{F}_i \cdot \mathbf{n}_{K,i} = \mathcal{F}_{KJ} \cdot \mathbf{n}_{K,i}, \quad (2.28)$$

where J is the cell where the boundary conditions are imposed, and \mathcal{F}_{KJ} is the two-points approximate Riemann solver chosen earlier.

- In the case where the mesh is admissible (see Definition 1.1), a lot of simplifications occur and the flux (2.26) becomes nothing but the two-points flux (2.10). In this case the coefficients previously defined are reduced to:

$$\begin{aligned} \mathcal{S}_{K,i} &= L & \bar{\mathcal{E}}_K &= \mathcal{E}_K \\ \beta_i &= 1 & \nu_{K,i}^{L,j} &= 1 \\ \gamma_{K,i}^j &= \gamma_{L,i}^j = \frac{1}{2} & d_L &= |e_i| \\ \omega_L^j &= \frac{|e_i|}{p_K} & \delta_{KL}^j &= \frac{|K|}{p_K}, \end{aligned}$$

with p_K the perimeter of the cell K , and j is the referring component in the system (1.2).

Moreover, the second condition of admissibility 2b of the Theorem 2.1 is immediately enforced.

2.4. Discussion on the choice of the flux

As it can be seen in (2.27), the property 2b does not hold on general meshes with the HLL-DLP flux, since $\sum_{i \in \mathcal{S}_{K,i}} \nu_{K,i}^{J,j} \boldsymbol{\eta}_{KJ} \neq \mathbf{n}_{K,i}$. This feature may be interpreted in a geometrical point of view (see Figure 6): property 2b would be true if the polygon constituted with the dash lines was closed. Unfortunately, this is not the case except for specific cases (e.g. for admissible meshes or when \mathbf{U} is constant over $\bar{\mathcal{E}}_K$).

Therefore, this property has to be enforced in order to use the Theorem 2.1 on general meshes. Moreover, the coefficients ν of the HLL-DLP flux (2.26) are defined by equations and not globally as in the Theorem 2.1. The preservation of \mathcal{A} thus cannot be guaranteed by Theorem 2.1.

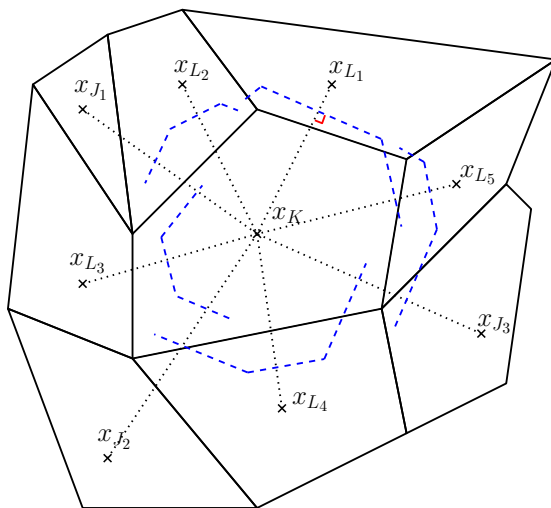


Figure 6: Virtual cell (in dashed blue), constituted with interfaces orthogonal to $\boldsymbol{\eta}_{KJ}$ with a length of d_{KJ} , which is not closed.

However, as a construction of a flux that fulfills all the conditions of the Theorem 2.1 and has diffusion on $\mathbf{n}_{K,i}$ ((i)) will be too cumbersome and numerically expensive, we may use a simpler procedure. Hence, we propose a method to conserve the set of admissible states \mathcal{A} , using an a posteriori limitation procedure, which may be used for high-order extensions (see [17] for instance). The scheme with the HLL-DLP flux (2.26) is used to compute the updates, then whenever this predicts a solution that is not admissible the TP flux (2.10) is used instead (see the Algorithm 1 for details about this procedure).

For practical implementation the following procedure, based on a posteriori criterion in the spirit of the MOOD paradigm used to develop high-order schemes [17], will hence be used (see also Figure 7):

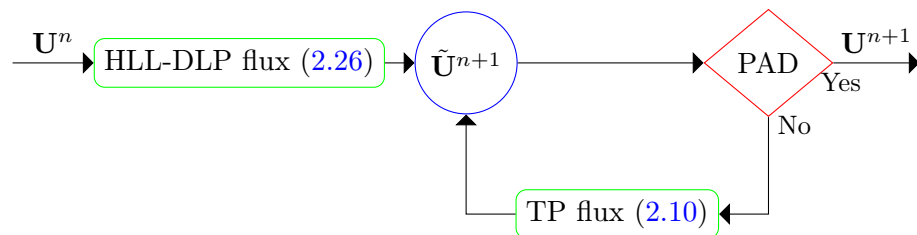


Figure 7: Principle of the TP correction

Such a correction is only expected to occur in the vicinity of discontinuities and on distorted cells, hence only few cells need to be corrected by this procedure. As it may be seen in the numerical results, this correction with the TP flux is seldom needed for classical test cases and the a posteriori procedure

Algorithm 1 Principle of the TP correction, with a Physical Admissibility Detector (PAD)

- 1: **procedure** TP-CORRECTION($\tilde{\mathbf{U}}^{n+1}$)
 - 2: * The computation of the candidates values $\tilde{\mathbf{U}}^{n+1}$ is done with the HLL-DLP flux (2.26) and with Δt given by the CFL condition (2.2) of the Theorem 2.1.
 - 3: **while** Physical Admissibility Detector: $(\exists K, \tilde{\mathbf{U}}_K^{n+1} \notin \mathcal{A})$ **do**
 - 4: * The property 2b of the Theorem 2.1 is enforced by using the TP flux (2.10) on all interfaces of all the cells K that do not satisfy the admissibility criterion. Therefore, this also modifies the values of $\tilde{\mathbf{U}}^{n+1}$ on all neighbors cells (to keep the conservation property). Then the time step and the new values of $\tilde{\mathbf{U}}^{n+1}$ are re-computed with the TP flux on the corrected cells (and their neighbors).
 - 5: **end while**
 - 6: **end procedure**
-

preserves a good precision.

Let us notice that there is no infinite loop in the procedure, as the TP flux satisfies all the properties of the Theorem 2.1 (see Section 2.2) and then conserves the set of admissible states. Let us also mention that the correction has no impact in the design of AP schemes in the next part. Indeed, it is proved in Lemma 3.3 and Corollary 3.1 that this correction with the two-points flux (2.10) is not activated when the AP property is required.

Finally, the scheme (2.1) with the HLL-DLP flux (2.26) is consistent, conservative and conserve the set of admissible states \mathcal{A} if the Algorithm 1 is used.

2.5. Numerical results for the hyperbolic scheme

The scheme (2.1) for the hyperbolic system without source term (1.2) is here validated on numerical tests. For the results with the source term the reader can refer to the Section 3.3.

2.5.1. Convergence results on the advection equation

In order to check the consistency of our numerical scheme, we test it on the advection equation:

$$\partial_t u + \operatorname{div}(\mathbf{a}u) = 0. \quad (2.29)$$

The test case is the transport at speed $\mathbf{a} = (1, 1)^T$ of a double sinus $u_0(x, y) = \sin(2\pi x) \sin(2\pi y)$ in a square $[0 ; 1]^2$. The square is meshed with an unstructured mesh presented in Figure 8, other meshes are refinement of this one. Even if, the coarse mesh is not distorted the refinements create some deformed cells. Dirichlet boundary conditions are imposed with the exact solution on each side of the square.

The L^2 -errors for the HLL-DLP flux (2.26) are presented at time $t_f = 1$ in the Table 1. They are compared to the errors with the TP flux (2.10) in the same table. The size of the mesh is defined as $\min_{K \in \mathcal{M}} \left(\frac{|K|}{\sum_{i \in \mathcal{E}_K} |e_i|} \right)$.

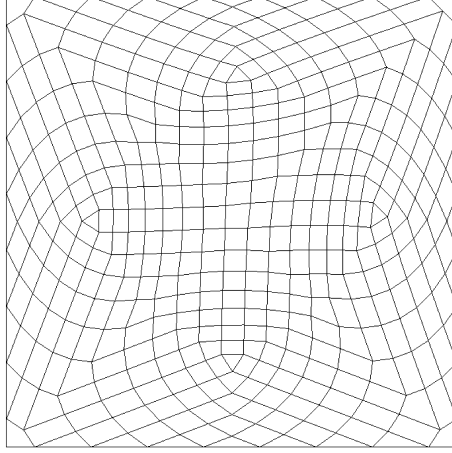


Figure 8: Coarser unstructured mesh used for the runs.

Mesh		HLL-DLP flux (2.26)		TP flux (2.10)	
Nb. cells	Size	Error	Order	Error	Order
1 569	2.67×10^{-3}	1.93×10^{-1}	—	2.01×10^{-1}	—
6 209	1.34×10^{-3}	1.19×10^{-1}	0.70	1.22×10^{-1}	0.72
24 705	6.68×10^{-4}	6.68×10^{-2}	0.83	6.83×10^{-2}	0.84
98 561	3.34×10^{-4}	3.58×10^{-2}	0.90	3.64×10^{-2}	0.91
393 729	1.67×10^{-4}	1.86×10^{-2}	0.95	1.89×10^{-2}	0.95
1 573 889	8.35×10^{-5}	9.49×10^{-3}	0.97	9.62×10^{-3}	0.97
6 293 505	4.17×10^{-5}	4.81×10^{-3}	0.98	4.97×10^{-3}	0.98

Table 1: Convergence rates.

Mesh		HLL-DLP-P0		HLL-DLP-P1		HLL-DLP-P2		HLL-DLP-P3	
Nb. cells	Size (Δx)	Error	Order	Error	Order	Error	Order	Error	Order
676	6.45E-03	2.24E-01	—	2.09E-02	—	1.36E-02	—	1.10E-03	—
2 704	3.22E-03	1.43E-01	0.65	4.19E-03	2.32	1.97E-03	2.79	7.58E-05	3.86
10 816	1.61E-03	8.25E-02	0.79	1.12E-03	1.90	2.82E-04	2.81	7.69E-06	3.30
43 264	8.06E-04	4.47E-02	0.89	3.14E-04	1.83	4.01E-05	2.82	5.00E-07	3.94
173 056	4.03E-04	2.33E-02	0.94	8.71E-05	1.85	5.44E-06	2.88	2.94E-08	4.09
692 224	2.01E-04	1.119E-02	0.97	2.49E-05	1.81	7.16E-07	2.92	1.91E-09	3.95

Table 2: Convergence rates with the double sinus

2.5.2. Sod's shock tube

The other test cases for this part are performed on the Euler model for ideal gases, which is nothing but (1.5) with the equation of conservation of the energy E and the following equation of state: $e = \frac{p}{\rho(\gamma-1)}$ (see [42] for a more detailed definition).

The first test case is Sod’s shock tube, which is a classical 1D test with possibility to compare with the exact solution of a 1D Riemann solver. This Riemann problem is characterised by a left state $\mathbf{U}_l = (1, 0, 0, 1)^T$, and a right states $\mathbf{U}_r = (0.125, 0, 0, 0.1)^T$. The results using the HLL-DLP flux, for different unstructured meshes are presented at time $t_f = 0.15$ in the Figure 9, with a section at $y = 0.5$. The convergence is observed on both the rarefaction waves

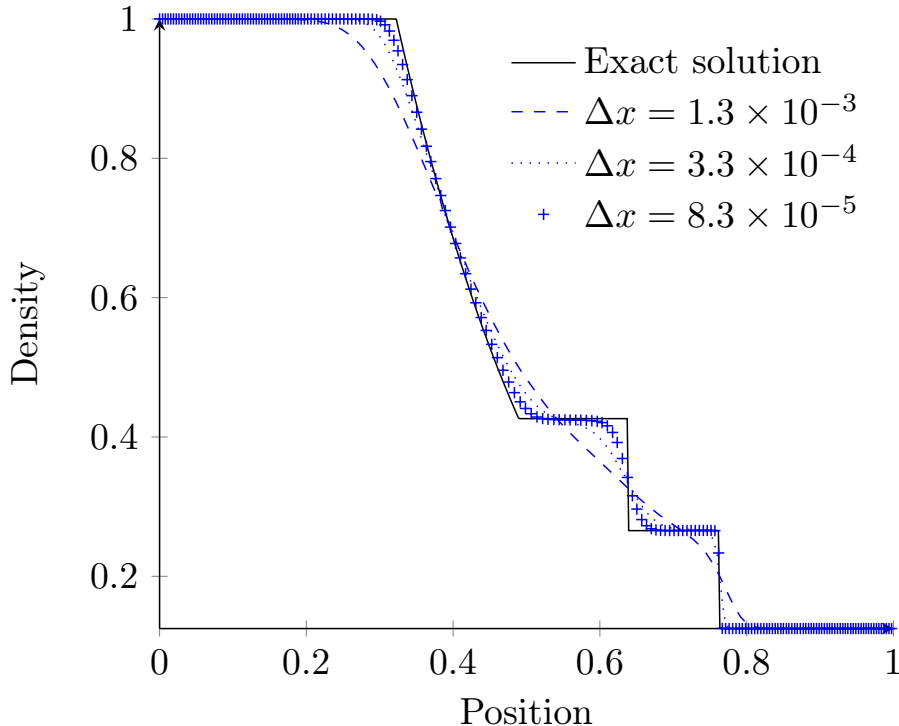


Figure 9: Density for the sod shock tube test case, solid line: exact solution; dashed line: coarse mesh (6.2×10^3 cells), dotted line: intermediary mesh (9.8×10^4 cells); and plus marks: fine mesh (1.5×10^6 cells).

and the shock. The contact discontinuity is logically not well described since only an HLL based scheme is used. The correction with the TP flux (2.10) is never used during the different runs, as the set of admissible states \mathcal{A} is always preserved during the computations. Hence, only the CPU time for the test of the physical admissibility is measured. For the three runs it costs less than 3% of the global computational time.

2.5.3. Wind tunnel at Mach 3

Another classical test case with the Euler model is the Mach 3 wind tunnel with a step from Woodward and Collela [44]. The computational domain and a coarse mesh are presented in Figure 10. The initial condition is a flow at Mach

3 with $\mathbf{U} = (1.4, 3, 0, 1)^T$, the same flow is imposed with Dirichlet boundary condition on the left side. The right side of the domain is a pressure outflow with Neumann boundary condition. Others surfaces are considered as walls.

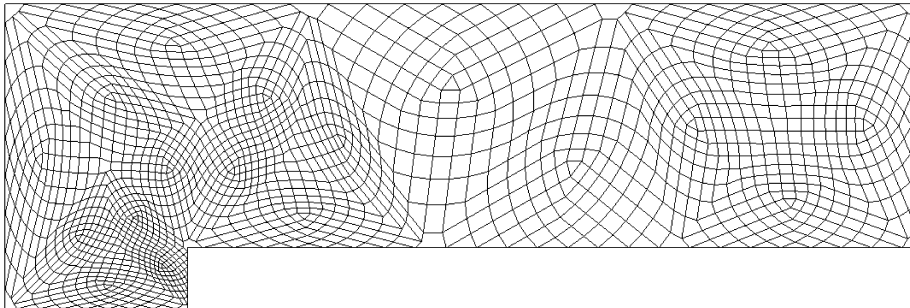


Figure 10: Prototype of unstructured mesh used for the computations in the tunnel.

In Figure 11 the solution on a coarse mesh of 1.7×10^3 cells with the two different fluxes (2.10) and (2.26) is presented in order to show the differences between the two fluxes. In the same figure the solution on a fine mesh of 1.7×10^6 cells with the HLL-DLP flux is given to have a comparison with the coarse mesh, moreover, this computation allow us to investigate the number of activations of the TP correction.

In the central figure (with the fine mesh) all the shocks and the different reflections are well captured. The difference between the TP flux (top figure) and the HLL-DLP flux (bottom figure) is observed by the different effects of the mesh on the solution. Since the numerical diffusion is only directed through KL with the TP flux, the flaws of the mesh are amplified, which is not the case with the scheme based on the HLL-DLP flux.

For both runs with the HLL-DLP flux, the TP flux correction is activated on less than 1% percent of the cells for a CPU cost inferior to 2% for the tests and the re-computations.

2.5.4. 2D Riemann problems

Other 2D test cases with reference solution with the Euler model are the 2D Riemann problems that were firstly introduced in [45], then corrected in [41] and simulated in [31].

The ones presented here are the third configuration (C3) which leads to the creation of four shocks and the fifth and sixth configurations (C5, C6) which deploy four contact discontinuities. The initial condition of these 2D Riemann problem is constituted of four states and described in Table 3.

The results for these test cases with an HLL based flux at time $t_f = 0.3$ are presented in Figure 12. These test cases are very sensitive to the initial condition, and that explains the form of the discontinuities as the initial condition is not properly aligned with the lines that divide the domain in four as the mesh is unstructured. The central structures are well represented in the three configurations, even with the unstructured mesh.

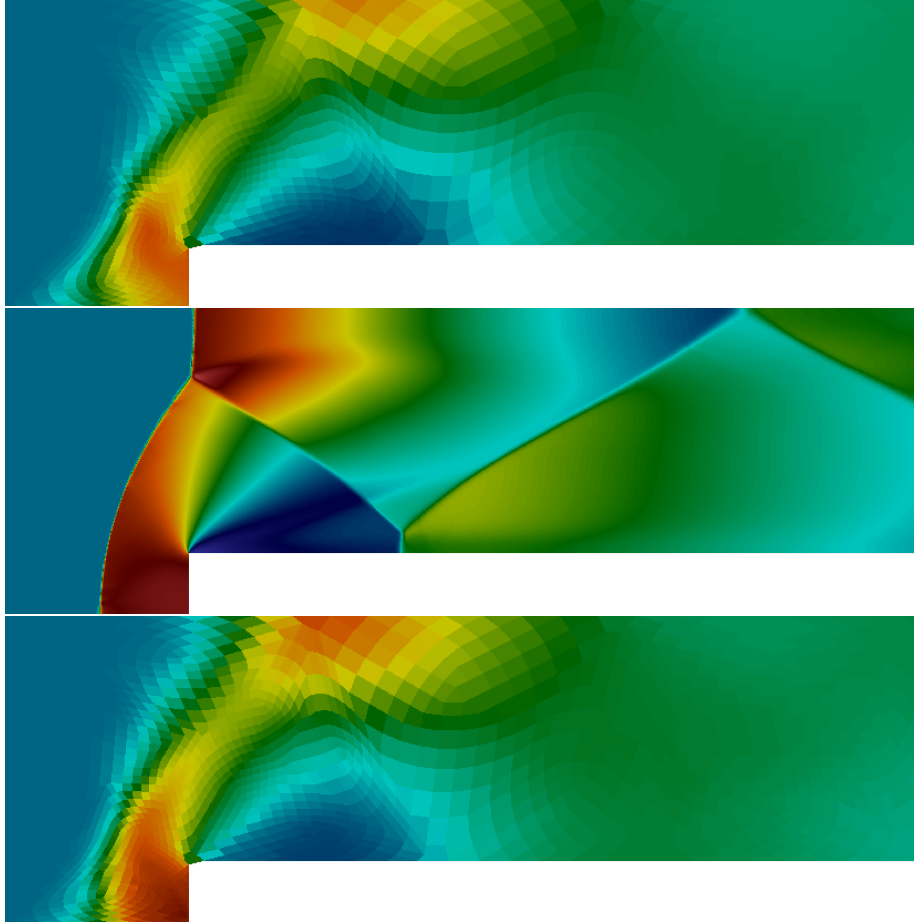


Figure 11: From top to bottom: density computed with the TP flux (2.10) on a coarse mesh, solution with the HLL-DLP flux (2.26) and the correction on a fine mesh of 1.7×10^6 cells, and solution on a coarse mesh with the HLL-DLP flux

The fifth and sixth configurations do not need any TP correction during the time iterations and the tests cost less than 1% of the CPU time. For the third configuration (the four shocks) the correction with the TP flux is used on less than 1% of the time iterations on a maximum of 5 cells with 3 loops (for the re-computations) in the procedure 1. The test for the physically admissible criterion and the re-computations only take 2% of the total CPU time.

2.5.5. 2D test case on the M_1 model

In order to prove that the scheme could be easily used on other hyperbolic systems of conservation laws as all the constructions are independent of the physical flux, we present a result with the M_1 model for radiative transfer described with (1.8).

	\mathbf{U}_{NW}^T				\mathbf{U}_{NE}^T			
	\mathbf{U}_{SW}^T				\mathbf{U}_{SE}^T			
C3	(0.5323	1.206	0.0	0.3)	(1.5	0.0	0.0	1.5)
	(0.138	1.206	1.206	0.029)	(0.5323	0.0	1.206	0.3)
C5	(2.0	-0.75	0.5	1.0)	(1.0	-0.75	-0.5	1.0)
	(1.0	0.75	0.5	1.0)	(3.0	0.75	-0.5	1.0)
C6	(2.0	0.75	0.5	1.0)	(1.0	0.75	-0.5	1.0)
	(1.0	-0.75	0.5	1.0)	(3.0	-0.750	-0.5	1.3)

Table 3: Four initial states for the configuration 3, 5 and 6 of the 2D Riemann problems for Euler (C3, C5, C6).

This test case is a 2D Riemann problem with four states inspired by those from the Euler equations. The initial condition is described by a temperature $T = 1000K$, a radiative energy $E = aT^4$ and a radiative flux $\mathbf{F}_R = (1 - 10^8)cE\mathbf{v}$ with \mathbf{v} defined as follows:

$\mathbf{v}_{NW} = \begin{pmatrix} 0 \\ 1 \end{pmatrix} \uparrow$	$\mathbf{v}_{NE} = \begin{pmatrix} -1 \\ 0 \end{pmatrix} \leftarrow$
$\mathbf{v}_{SW} = \begin{pmatrix} 1 \\ 0 \end{pmatrix} \rightarrow$	$\mathbf{v}_{SE} = \begin{pmatrix} 0 \\ -1 \end{pmatrix} \downarrow$

This test case is very stiff as $f = \frac{\|\mathbf{F}_R\|}{cE}$ stays close to 1 in most of the domain during the time iterations, and the initial condition itself is close to the boundary of the set of admissible states \mathcal{A} .

The results for the radiative energy and the factor of anisotropy f at time $t_f = 2 \times 10^{-9}$ are presented in Figure 13. As f stays near 1 during all the computations and in a major part of the domain, the TP correction could have been expected. Moreover, strong discontinuities appear in the center of the domain. In fact, less than 1% of the cells are corrected at each iteration within less than 5% of the total CPU time due to the loops for the re-computations in the Algorithm 1.

Finally, the HLL-DLP (2.26) flux and the procedure associated to preserve the set of admissible states \mathcal{A} (1) for the hyperbolic homogeneous system (1.2) are well suited on classical test cases and even for very stiff ones.

3. Numerical scheme for the system of conservation laws with source term

Now we design a scheme for the full system of conservation law with source term (1.1). This scheme is based on the scheme for the hyperbolic part introduced in the previous part (2.1) and will be proved to be AP with the diffusion

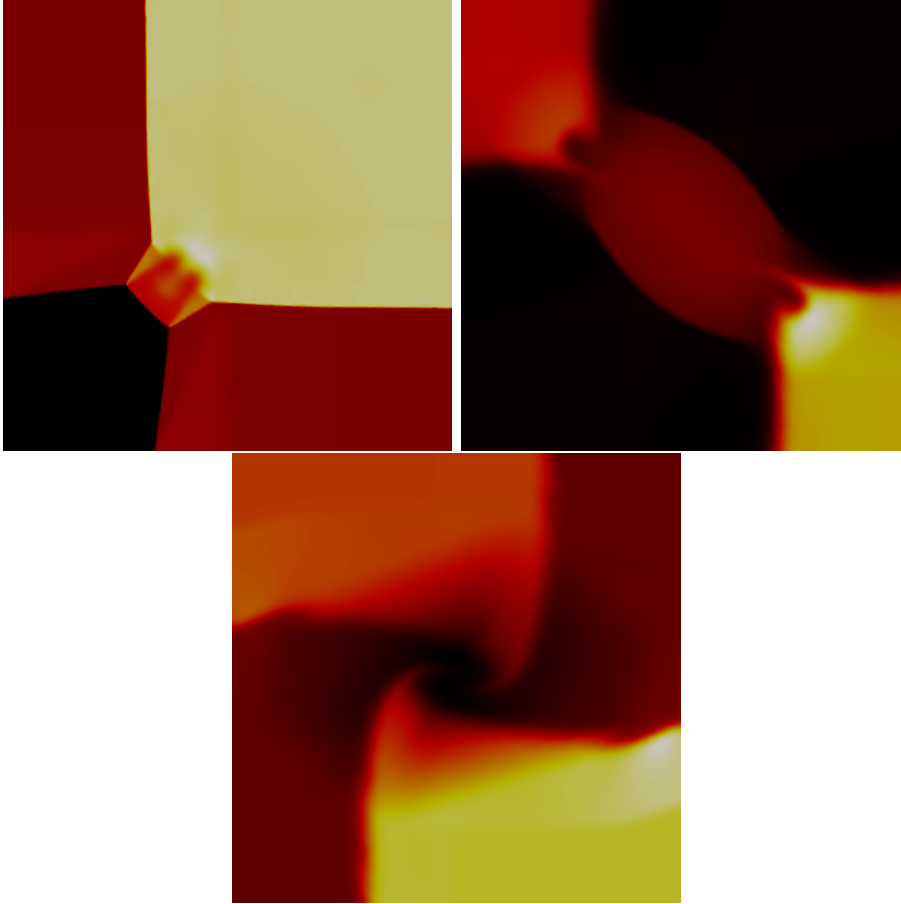


Figure 12: Density results for three 2D Riemann problems on an unstructured mesh with 1.2×10^6 cells.

limit (1.4). For the sake of simplicity it is exposed under the following form:

$$\forall K \in \mathcal{M}, \mathbf{U}_K^{n+1} = \mathbf{U}_K^n - \frac{\Delta t}{|K|} \sum_{i \in \mathcal{E}_K} |e_i| \overline{\mathcal{F}}_{K,i} \cdot \mathbf{n}_{K,i}, \quad (3.1)$$

where the flux $\overline{\mathcal{F}}_{K,i}$ contains the discretization of both the hyperbolic part and the source term from (1.1). Naturally, the objective is to design an expression of $\overline{\mathcal{F}}_{K,i}$ which also preserves the set of admissible states \mathcal{A} .

3.1. Construction of $\overline{\mathcal{F}}_{K,i}$

Now that a relevant scheme has been designed for the hyperbolic part, we propose to modify it in order to take the source term into account using the technique introduced in [7] for the 1D case (see also [6, 22] for the introduction in 2D).

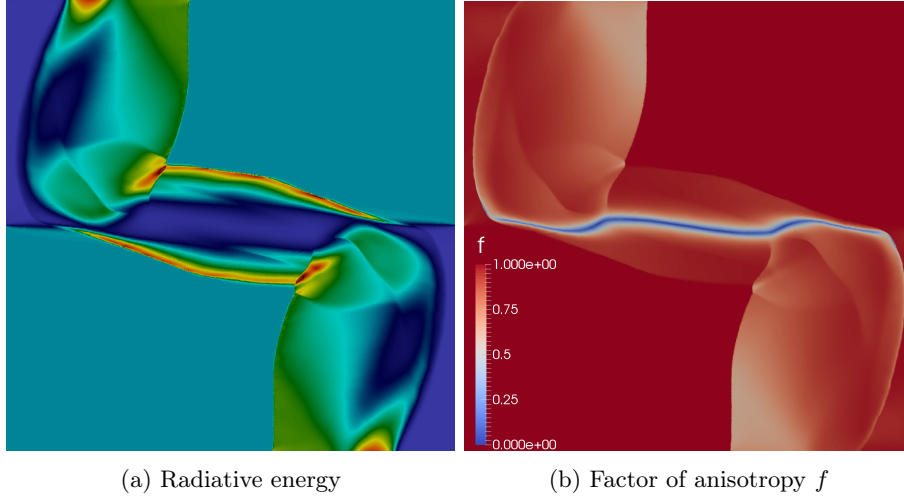


Figure 13: Results for a 2D Riemann problems on an unstructured mesh of 1.2×10^6 cells with the M_1 model

This modification can be easily done as all the three points (i)-(ii)-(iii) required are respected by the scheme with the HLL-DLP flux.

In order to reuse the convex combinations used in the proof of the Theorem 2.1, the modification is applied in the direction KJ as follows:

$$\begin{aligned} \bar{\mathcal{F}}_{KJ} \cdot \boldsymbol{\eta}_{KJ} &= \alpha_{KJ} \mathcal{F}_{KJ} \cdot \boldsymbol{\eta}_{KJ} - (\alpha_{KJ} - \alpha_{KK}) \mathbf{F}(\mathbf{U}_K^n) \cdot \boldsymbol{\eta}_{KJ} \\ &\quad - (1 - \alpha_{KJ}) b_{KJ} (\mathbf{R}(\mathbf{U}_K^n) - \mathbf{U}_K^n), \end{aligned} \quad (3.2)$$

where \mathcal{F}_{KJ} is a two-points approximate Riemann solver, for instance the Rusanov flux as in (2.15) (see Appendix D for the changes implied by the HLL flux), and the α coefficients are defined by components j as:

$$\begin{cases} (\alpha_{KJ})^j &= \alpha_{KJ}^j = \frac{b_{KJ}}{b_{KJ} + \gamma_K \delta_{KJ}^j} \in [0; 1], \\ \alpha_{KK} &= \frac{b_{KK}}{b_{KK} + \gamma_K \delta_{KK}}, \text{ with } \delta_{KK} = \frac{|K|}{p_K}, \end{cases} \quad (3.3)$$

where $\gamma_K = \gamma(\mathbf{U}_K^n)$, and $\delta_{KJ}^j = \frac{|K|}{\sum_{J \in \bar{\mathcal{E}}_K} d_{KJ}^j}$, with $d_{KJ}^j = \sum_{i \in \mathcal{S}_{K,i}} |e_i| \nu_{K,i}^{J,j}$. The coefficients ν are computed on \mathcal{F}_{KJ} as previously in (2.26).

Now the flux $\bar{\mathcal{F}}_{K,i}$ is also reconstructed from the modified 1D fluxes (3.2):

$$\bar{\mathcal{F}}_{K,i} \cdot \mathbf{n}_{K,i} = \sum_{J \in \mathcal{S}_{K,i}} \nu_{K,i}^J \bar{\mathcal{F}}_{KJ} \cdot \boldsymbol{\eta}_{KJ}, \quad (3.4)$$

where $\nu_{K,i}^J = (\nu_{K,i}^{J,j})_j$ is obtained as previously on \mathcal{F}_{KJ} in the Section 2.3.

The HLL-DLP scheme (3.1) hence becomes:

$$\begin{aligned}
\mathbf{U}_K^{n+1} &= \mathbf{U}_K^n - \frac{\Delta t}{|K|} \sum_{i \in \mathcal{E}_K} |e_i| \sum_{J \in \mathcal{S}_{K,i}} \nu_{K,i}^J \overline{\mathcal{F}}_{KJ} \cdot \boldsymbol{\eta}_{KJ} \\
&= \mathbf{U}_K^n - \frac{\Delta t}{|K|} \sum_{i \in \mathcal{E}_K} |e_i| \sum_{J \in \mathcal{S}_{K,i}} \nu_{K,i}^J (\boldsymbol{\alpha}_{KJ} \mathcal{F}_{KJ} \cdot \boldsymbol{\eta}_{KJ} \\
&\quad - (\boldsymbol{\alpha}_{KJ} - \boldsymbol{\alpha}_{KK}) \mathbf{F}(\mathbf{U}_K^n) \cdot \boldsymbol{\eta}_{KJ}) \\
&\quad + \frac{\Delta t}{|K|} \sum_{i \in \mathcal{E}_K} |e_i| \sum_{J \in \mathcal{S}_{K,i}} \nu_{K,i}^J (1 - \boldsymbol{\alpha}_{KJ}) b_{KJ} (\mathbf{R}(\mathbf{U}_K^n) - \mathbf{U}_K^n)
\end{aligned} \tag{3.5}$$

In order to preserve the set of admissible states \mathcal{A} we generalise the Theorem 2.1 by including the source term with the flux $\overline{\mathcal{F}}_{K,i}$.

Theorem 3.1. *The scheme (3.1) expanded in (3.5) is consistent with (1.1), under the same assumptions of the Theorem 2.1. Moreover, it preserves the set of admissible states \mathcal{A} under the CFL condition:*

$$\max_{\substack{K \in \mathcal{M} \\ J \in \overline{\mathcal{E}}_K}} \left(b_{KJ} \frac{\Delta t}{\delta_{KJ}} \right) \leq 1. \tag{2.2}$$

Proof. First we use two lemmas to prove the consistency:

Lemma 3.1. *The term $\sum_{J \in \mathcal{S}_{K,i}} \nu_{K,i}^J (\boldsymbol{\alpha}_{KJ} \mathcal{F}_{KJ} \cdot \boldsymbol{\eta}_{KJ} - (\boldsymbol{\alpha}_{KJ} - \boldsymbol{\alpha}_{KK}) \mathbf{F}(\mathbf{U}_K^n) \cdot \boldsymbol{\eta}_{KJ})$ of (3.5) is consistent with $\mathbf{F}(\mathbf{U}) \cdot \mathbf{n}_{K,i}$.*

Proof. One can assume that $\nu_{K,i}^J \leq C$, with $C \in [0; +\infty[$. Then when the radius of the largest circle inside K , r_K , tends to zero we have:

$$\delta_{KJ} = \frac{|K|}{\sum_{J \in \overline{\mathcal{E}}_K} d_{KJ}} = \frac{|K|}{\sum_{i \in \mathcal{E}_K} |e_i| \sum_{J \in \mathcal{S}_{K,i}} \nu_{K,i}^J} \rightarrow 0.$$

Next, from the definition of $\boldsymbol{\alpha}_{KJ}$ and $\boldsymbol{\alpha}_{KK}$ we have $\boldsymbol{\alpha}_{KJ} \xrightarrow[r_K \rightarrow 0]{} 1$ and $\boldsymbol{\alpha}_{KK} \xrightarrow[r_K \rightarrow 0]{} 1$.

Now, since $\sum_{J \in \mathcal{S}_{K,i}} \nu_{K,i}^J \mathcal{F}_{KJ} \cdot \boldsymbol{\eta}_{KJ}$ is consistent with $\mathbf{F}(\mathbf{U}) \cdot \mathbf{n}_{K,i}$ (as stated in the previous section), those terms are consistent with $\mathbf{F}(\mathbf{U}) \cdot \mathbf{n}_{K,i}$. \square

Lemma 3.2. *The term that discretizes the source term in (3.5):*

$$\mathbf{S}(\mathbf{U}_K^n) := \sum_{i \in \mathcal{E}_K} \frac{|e_i|}{|K|} \left(\sum_{J \in \mathcal{S}_{K,i}} \nu_{K,i}^J (1 - \boldsymbol{\alpha}_{KJ}) b_{KJ} (\mathbf{R}(\mathbf{U}_K^n) - \mathbf{U}_K^n) \right),$$

is consistent with $\gamma(\mathbf{U})(\mathbf{R}(\mathbf{U}) - \mathbf{U})$.

Proof. Inverting the two sums, and using the definition of ω_{KJ} and δ_{KJ} we have:

$$\begin{aligned}
\mathbf{S}(\mathbf{U}_K^n) &= \sum_{J \in \bar{\mathcal{E}}_K} \left(\frac{\omega_{KJ}}{\delta_{KJ}} (1 - \alpha_{KJ}) b_{KJ} (\mathbf{R}(\mathbf{U}_K^n) - \mathbf{U}_K^n) \right) \\
&= \sum_{J \in \bar{\mathcal{E}}_K} \left(\frac{\omega_{KJ}}{\delta_{KJ}} \frac{\gamma_K \delta_{KJ}}{b_{KJ} + \gamma_K \delta_{KJ}} b_{KJ} (\mathbf{R}(\mathbf{U}_K^n) - \mathbf{U}_K^n) \right) \\
&= \gamma_K (\mathbf{R}(\mathbf{U}_K^n) - \mathbf{U}_K^n) \sum_{J \in \bar{\mathcal{E}}_K} \left(\omega_{KJ} \frac{b_{KJ}}{b_{KJ} + \gamma_K \delta_{KJ}} \right)
\end{aligned}$$

Therefore, as $\delta_{KJ} \xrightarrow{r_K \rightarrow 0} 0$, we have:

$$\sum_{J \in \bar{\mathcal{E}}_K} \left(\omega_{KJ} \frac{b_{KJ}}{b_{KJ} + \gamma_K \delta_{KJ}} \right) \xrightarrow{r_K \rightarrow 0} \sum_{J \in \bar{\mathcal{E}}_K} \omega_{KJ} = 1.$$

□

Then to prove the stability under a CFL condition the scheme is rewritten as a convex combination of 1D schemes from [7]. By inverting all the sums in (3.5) we have:

$$\begin{aligned}
\mathbf{U}_K^{n+1} &= \mathbf{U}_K^n - \frac{\Delta t}{|K|} \sum_{i \in \mathcal{E}_K} |e_i| \bar{\mathcal{F}}_{K,i} \cdot \mathbf{n}_{K,i} \\
&= \mathbf{U}_K^n - \sum_{J \in \bar{\mathcal{E}}_K} \left(\omega_{KJ} \frac{\Delta t}{\delta_{KJ}} \alpha_{KJ} \mathcal{F}_{KJ} \cdot \boldsymbol{\eta}_{KJ} \right) \\
&\quad + \sum_{J \in \bar{\mathcal{E}}_K} \left(\omega_{KJ} \frac{\Delta t}{\delta_{KJ}} (\alpha_{KJ} - \alpha_{KK}) \mathbf{F}(\mathbf{U}_K^n) \cdot \boldsymbol{\eta}_{KJ} \right) \\
&\quad + \sum_{J \in \bar{\mathcal{E}}_K} \left(\omega_{KJ} \frac{\Delta t}{\delta_{KJ}} (1 - \alpha_{KJ}) b_{KJ} (\mathbf{R}(\mathbf{U}_K^n) - \mathbf{U}_K^n) \right)
\end{aligned} \tag{3.6}$$

The assumption 2b of the Theorem 2.1 gives:

$$\begin{aligned}
0 &= \sum_{J \in \bar{\mathcal{E}}_K} \omega_{KJ} \frac{\Delta t}{\delta_{KJ}} \alpha_{KK} \mathcal{F}_{KK} \cdot \boldsymbol{\eta}_{KJ} \\
0 &= \sum_{J \in \bar{\mathcal{E}}_K} \omega_{KJ} \frac{\Delta t}{\delta_{KJ}} (1 - \alpha_{KK}) b_{KK} (\mathbf{R}(\mathbf{U}_K^n) - \mathbf{U}_K^n)
\end{aligned} \tag{3.7}$$

The term $\sum_{J \in \bar{\mathcal{E}}_K} \omega_{KJ} \frac{\Delta t}{\delta_{KJ}} (1 - \alpha_{KK}) b_{KK} (\mathbf{R}(\mathbf{U}_K^n) - \mathbf{U}_K^n)$ is equal to zero because it may be rewritten using the equality $\mathbf{R}(\mathbf{U}_K^n) - \mathbf{U}_K^n = \mathbf{S}_{KK} \cdot \boldsymbol{\eta}_{KJ}$.

With the addition of the terms from (3.7) the previous scheme can be rewritten as:

$$\begin{aligned}
\mathbf{U}_K^{n+1} &= \sum_{J \in \bar{\mathcal{E}}_K} \omega_{KJ} \left(\mathbf{U}_K^n - \frac{\Delta t}{\delta_{KJ}} [\alpha_{KJ} \mathcal{F}_{KJ} - \alpha_{KK} \mathcal{F}_{KK}] \cdot \boldsymbol{\eta}_{KJ} \right. \\
&\quad + \frac{\Delta t}{\delta_{KJ}} [\alpha_{KJ} \mathbf{F}(\mathbf{U}_K^n) - \alpha_{KK} \mathbf{F}(\mathbf{U}_K^n)] \cdot \boldsymbol{\eta}_{KJ} \\
&\quad \left. + \frac{\Delta t}{\delta_{KJ}} [(1 - \alpha_{KJ}) - (1 - \alpha_{KK})] b_{KK} (\mathbf{R}(\mathbf{U}_K^n) - \mathbf{U}_K^n) \right) \\
&= \sum_{J \in \bar{\mathcal{E}}_K} \omega_{KJ} \left(\mathbf{U}_K^n - \frac{\Delta t}{\delta_{KJ}} [\tilde{\mathcal{F}}_{KJ} - \tilde{\mathcal{F}}_{KK}] \cdot \boldsymbol{\eta}_{KJ} \right)
\end{aligned} \tag{3.8}$$

$$\tag{3.9}$$

This last scheme (3.9) is a convex combination of 1D scheme with $\tilde{\mathcal{F}}_{KJ}$ as numerical flux:

$$\begin{aligned}
\tilde{\mathcal{F}}_{KJ} \cdot \boldsymbol{\eta}_{KJ} &= \alpha_{KJ} \mathcal{F}_{KJ} \cdot \boldsymbol{\eta}_{KJ} - \alpha_{KJ} \mathbf{F}(\mathbf{U}_K^n) \cdot \boldsymbol{\eta}_{KJ} \\
&\quad - (1 - \alpha_{KJ}) b_{KJ} (\mathbf{R}(\mathbf{U}_K^n) - \mathbf{U}_K^n),
\end{aligned} \tag{3.10}$$

and for the intermediary state:

$$\begin{aligned}
\tilde{\mathcal{F}}_{KK} \cdot \boldsymbol{\eta}_{KJ} &= \alpha_{KK} \mathcal{F}_{KK} \cdot \boldsymbol{\eta}_{KJ} - \alpha_{KK} \mathbf{F}(\mathbf{U}_K^n) \cdot \boldsymbol{\eta}_{KJ} \\
&\quad - (1 - \alpha_{KK}) b_{KK} (\mathbf{R}(\mathbf{U}_K^n) - \mathbf{U}_K^n).
\end{aligned} \tag{3.11}$$

These flux $\tilde{\mathcal{F}}$ are these defined in [7], and then are stable under the CFL condition:

$$\max_{\substack{K \in \mathcal{M} \\ J \in \bar{\mathcal{E}}_K}} \left(b_{KJ} \frac{\Delta t}{\delta_{KJ}} \right) \leq 1. \tag{2.2}$$

In addition, they have the right AP properties. \square

Remark 3.1. *As this theorem is a generalisation of the previous Theorem 2.1, the proof is only done with a scalar $\nu_{K,i}^J$.*

Let us recall that the scheme with source term (3.1) is a direct extension of the scheme for the hyperbolic system (2.1), built using the method from [7]. Thus, this new scheme does not fulfill all the assumptions of the theorem and the same TP flux correction described in Algorithm 1 is mandatory to preserve the set of admissible states \mathcal{A} . Before presenting the AP preserving correction for the scheme (3.1), Lemma 3.3 and Corollary 3.1 prove that the TP flux correction is not needed in the diffusive limit and will not modify the numerical diffusion needed for the AP property.

Lemma 3.3. *In the diffusion limit, Theorem 3.1 is valid under the assumptions 1 and 2a (property 2b is not required in that case): the scheme (3.1) preserves the set of admissible states under the CFL condition (2.2).*

Proof. In the proof of Theorem 3.1, property 2b was only used to enforce the two relations labeled (3.7). In the diffusive limit, \mathbf{U} lies in the equilibrium map defined by the compatibility conditions (see [5]). In particular, the two relations (3.7) are true on the equilibrium map, since:

1. $\mathbf{QF}(\mathbf{U}) = 0$ on the equilibrium map (see property (1.7) in [5]), where \mathbf{Q} is the constant $1 \times N$ matrix that multiplies the system (1.1) to obtain the limit diffusion equation (1.4). This is indeed crucial for systems in the form of (1.1) to fulfill this property in order to degenerate into diffusion equation as stated in [5].
2. $\mathbf{R}(\mathbf{U}) = \mathbf{U}$ is part of the definition of the equilibrium map (see property (1.4) in [5]).

Therefore (3.7) is true on the equilibrium map independently of property 2b. Consequently, it is also true in the diffusive limit. The rest of the proof of Theorem 3.1 is not modified. \square

Corollary 3.1. *The correction with the TP flux (2.10) described in the Algorithm 1 is never active in the diffusion limit.*

Proof. In the diffusive limit, only one scalar $\nu_{K,i}^J$ is involved in the numerical scheme since only scalar diffusion limits are considered in this paper.

Now, using Lemma 3.3, the scheme (3.1) enters the framework of Theorem 3.1 in the diffusion limit. Therefore, it preserves the set of admissible states in this situation. \square

3.2. Asymptotic limit of the scheme

Now the asymptotic behaviour (when $\gamma(\mathbf{U})t \rightarrow \infty$) of the scheme (3.1) is investigated. To do so, a formal Champagn-Enskog expansion [7, 6] is performed by introducing $\varepsilon > 0$ with the following rescaling:

$$\begin{cases} \gamma & \leftarrow \frac{\gamma}{\varepsilon} \\ \Delta t & \leftarrow \frac{\Delta t}{\varepsilon} \end{cases}$$

In the continuous case, this restrictive rescaling leads to the right limit to the diffusion equation [5], and it also provides the expected limit with discrete computations. It is therefore used to investigate the AP property of numerical schemes since the rigorous arguments used in the continuous case are not adapted to numerical schemes.

The following expansions can be deduced from this rescaling, with j the index of the component in the system (1.1):

$$\begin{cases} \Delta t \alpha_{KJ}^j & = \Delta t \frac{b_{KJ}}{b_{KJ}\varepsilon + \gamma_K \delta_{KJ}^j} & = \Delta t \frac{b_{KJ}}{\gamma_K \delta_{KJ}^j} + o(1) \\ \Delta t \alpha_{KK} & = \Delta t \frac{b_{KK}}{b_{KK}\varepsilon + \gamma_K \delta_{KK}} & = \Delta t \frac{b_{KK}}{\gamma_K \delta_{KK}} + o(1) \\ \Delta t (1 - \alpha_{KJ}^j) & = \Delta t \frac{\gamma_K \delta_{KJ}^j}{b_{KJ}\varepsilon^2 + \gamma_K \delta_{KJ}^j \varepsilon} & = \frac{\Delta t}{\varepsilon} + o(\varepsilon) \end{cases}$$

By reintroducing this expansion in the scheme (3.5) and identifying terms in ε^{-1} the equilibrium is obtained:

$$\mathbf{R}(\mathbf{U}) = \mathbf{U}. \quad (3.12)$$

Now, the ε^0 terms yield:

$$\mathbf{U}_K^{n+1,j} = \mathbf{U}_K^{n,j} - \sum_{i \in \mathcal{E}_K} \frac{\Delta t}{|K|} |e_i| \sum_{J \in \mathcal{S}_{K,i}} \frac{\nu_{K,i}^{J,j}}{\gamma_K} \left[\frac{b_{KJ}}{\delta_{KJ}^j} \mathcal{F}_{KJ}^j - \left(\frac{b_{KJ}}{\delta_{KJ}^j} - \frac{b_{KK}}{\delta_{KK}} \right) \mathbf{F}^j(\mathbf{U}_K^n) \right] \cdot \boldsymbol{\eta}_{KJ} \Big|_{\mathbf{R}(\mathbf{U})=\mathbf{U}} \quad (3.13)$$

As usual with the technique of [7] the scheme is not generally AP at this point. The asymptotic property is recovered by introducing a free parameter $\bar{\gamma}$ such as $\gamma + \bar{\gamma} > 0$:

$$\partial_t \mathbf{U} + \text{div}(\mathbf{F}(\mathbf{U})) = \gamma(\mathbf{U})(\mathbf{R}(\mathbf{U}) - \mathbf{U}), \quad (3.11)$$

$$= \gamma(\mathbf{U})(\mathbf{R}(\mathbf{U}) - \mathbf{U}) + (\bar{\gamma} - \bar{\gamma})\mathbf{U},$$

$$\partial_t \mathbf{U} + \text{div}(\mathbf{F}(\mathbf{U})) = (\gamma(\mathbf{U}) + \bar{\gamma})(\bar{\mathbf{R}}(\mathbf{U}) - \mathbf{U}), \quad (3.14)$$

with the following relation:

$$\bar{\mathbf{R}}(\mathbf{U}) = \frac{\gamma(\mathbf{U})\mathbf{R} + \bar{\gamma}\mathbf{U}}{\gamma(\mathbf{U}) + \bar{\gamma}} \in \mathcal{A}. \quad (3.15)$$

The scheme (3.1) is now applied on this equivalent system (3.14) and $\bar{\gamma}$ turns out to be a free parameter that can be chosen to obtain an asymptotic scheme for (1.1). Then, the identification of the ε^0 terms as in (3.13), becomes:

$$\mathbf{U}_K^{n+1,j} = \mathbf{U}_K^{n,j} - \sum_{i \in \mathcal{E}_K} \frac{\Delta t}{|K|} |e_i| \sum_{J \in \mathcal{S}_{K,i}} \frac{\nu_{K,i}^{J,j}}{\gamma_K + \bar{\gamma}_{K,i}^J} \left[\frac{b_{KJ}}{\delta_{KJ}^j} \mathcal{F}_{KJ}^j - \left(\frac{b_{KJ}}{\delta_{KJ}^j} - \frac{b_{KK}}{\delta_{KK}} \right) \mathbf{F}^j(\mathbf{U}_K^n) \right] \cdot \boldsymbol{\eta}_{KJ} \Big|_{\mathbf{R}(\mathbf{U})=\mathbf{U}}. \quad (3.16)$$

The way to choose a relevant expression of $\bar{\gamma}$ is illustrated on the two systems presented in the introduction (1.5) and (1.8) with a Rusanov based flux. The computations are done similarly for others fluxes or system of conservation laws (see for instance Appendix D for the computations done with an HLL based flux on these systems)

3.2.1. Limit scheme for the Euler equations with friction

For the Euler model (1.5) the equilibrium $\mathbf{R}(\mathbf{U}) = \mathbf{U}$ implies $\rho_u = \rho_v = 0$. Denoting $\gamma + \bar{\gamma} := \kappa + \bar{\kappa}$, to stay consistent with the usual notations, we have the following limit scheme:

$$\rho_K^{n+1} = \rho_K^n + \sum_{i \in \mathcal{E}_K} \frac{\Delta t}{|K|} |e_i| \sum_{J \in \mathcal{S}_{K,i}} \nu_{K,i}^{J,\rho} \frac{b_{KJ}^2}{2(\kappa_K + \bar{\kappa}_{K,i}^J) \delta_{KJ}^\rho} (\rho_J - \rho_K). \quad (3.17)$$

The free parameter $\bar{\kappa}$ is chosen such that:

$$\frac{\nu_{K,i}^{J,\rho} b_{KJ}^2}{2(\kappa_K + \bar{\kappa}_{K,i}^J) \delta_{KJ}^\rho} (\rho_J - \rho_K) = \frac{\bar{\nu}_{K,i}^J}{\kappa_K} (p_J - p_K), \quad (3.18)$$

which leads to:

$$\bar{\kappa}_{K,i}^J = \begin{cases} \kappa_K \left(\frac{\nu_{K,i}^{J,\rho} b_{KJ}^2}{2\bar{\nu}_{K,i}^J \delta_{KJ}^\rho} \frac{\rho_J - \rho_K}{p_J - p_K} - 1 \right), & \text{if } p_J \neq p_K \\ \kappa_K \left(\frac{\nu_{K,i}^{J,\rho} b_{KJ}^2}{2\bar{\nu}_{K,i}^J \delta_{KJ}^\rho} \frac{1}{p'(\rho_K)} - 1 \right), & \text{otherwise} \end{cases} \quad (3.19)$$

where $\bar{\nu}_{K,i}^J$ is the coefficient of the DLP scheme developed in [20] computed on the diffusion equation (1.7).

Remark 3.2.

- The coefficients $\kappa_K + \bar{\kappa}_{K,i}^J$ are positive as $p'(\rho) > 0$ and all the ν and $\bar{\nu}$ coefficients are positive by construction.
- If $\nu_{K,i}^{J,\rho}$ or $\bar{\nu}_{K,i}^J$ is equal to zero, then the asymptotic correction $\bar{\kappa}_{K,i}^J$ is set to zero. This may happen during the computations but never in the diffusive limit.

With the correction (3.19) the limit scheme is now:

$$\rho_K^{n+1} = \rho_K^n + \sum_{i \in \mathcal{E}_K} \frac{\Delta t}{|K|} |e_i| \sum_{J \in \mathcal{S}_{K,i}} \frac{\bar{\nu}_{K,i}^J}{\kappa_K} (p_J - p_K), \quad (3.20)$$

which is nothing but the DLP scheme for:

$$\partial_t(\rho) - \operatorname{div} \left(\frac{1}{\kappa} \nabla p \right) = 0. \quad (1.7)$$

3.2.2. Limit scheme for the M_1 model

For the M_1 model (1.8) the equilibrium $\mathbf{R}(\mathbf{U}) = \mathbf{U}$ implies that $E = aT^4$, and $\mathbf{F}_R = 0$. Setting $b_{KJ} = c$ (see [34, 2]), and $\gamma + \bar{\gamma} := c(\sigma^m + \bar{\sigma}^m)$ we have the following limit scheme:

$$\begin{aligned} (\rho C_v T + aT^4)_K^{n+1} &= (\rho C_v T + aT^4)_K^n \\ &+ \sum_{i \in \mathcal{E}_K} \frac{\Delta t}{|K|} |e_i| \sum_{J \in \mathcal{S}_{K,i}} \nu_{K,i}^{J,E} \frac{c}{2((\sigma^m)_K + (\bar{\sigma}^m)_{K,i}^J) \delta_{KJ}^E} ((aT^4)_J - (aT^4)_K). \end{aligned} \quad (3.21)$$

The parameter $\bar{\sigma}^m$ is chosen such that:

$$\frac{\nu_{K,i}^{J,E}}{2((\sigma^m)_K + (\bar{\sigma}^m)_{K,i}^J) \delta_{KJ}^E} = \frac{\bar{\nu}_{K,i}^J}{3(\sigma^f)_K}, \quad (3.22)$$

which leads to:

$$(\bar{\sigma}^m)^J_{K,i} = 3(\sigma^f)_K \frac{\nu_{K,i}^{J,E}}{2\bar{\nu}_{K,i}^J \delta_{KJ}} - (\sigma^m)_K. \quad (3.23)$$

With the choice (3.23) the limit scheme is now:

$$\begin{aligned} (\rho C_v T + aT^4)_K^{n+1} &= (\rho C_v T + aT^4)_K^n \\ &+ \sum_{i \in \mathcal{E}_K} \frac{\Delta t}{|K|} |e_i| \sum_{J \in \mathcal{S}_{K,i}} \bar{\nu}_{K,i}^J \frac{c}{3(\sigma^f)_K} ((aT^4)_J - (aT^4)_K), \end{aligned} \quad (3.24)$$

which is the DLP scheme for the asymptotic limit of the M_1 model (the *equilibrium diffusion equation*):

$$\partial_t (\rho C_v T + aT^4) - \operatorname{div} \left(\frac{c}{3\sigma^f} \nabla (aT^4) \right) = 0. \quad (1.10)$$

Remark 3.3. *This asymptotic correction is linked to the fact that we choose to set the numerical flux on the fourth equation of the M_1 model to zero, $\mathcal{F}_i^T = 0$, as the physical flux \mathbf{F} is equal to zero in this equation and T is only coupled with (E, \mathbf{F}_R) through the source term.*

3.3. Numerical results for the scheme with source term

3.3.1. Pseudo 1D continuous test case

The first test case to check the asymptotic behaviour of the scheme (3.1), is a pseudo 1D test case on the M_1 model with the following properties: all the opacities (σ^a , σ^e , σ^f) are fixed to 1500 and the initial condition is a Gaussian in temperature $T_0(x) = 300 \exp\left(-\frac{(x-0.5)^2}{2 \times 0.05^2}\right) + 300$, and in order to be at the radiative equilibrium $E_0 = aT_0^4$ and $\mathbf{F}_{R,0} = 0$.

The solution with the scheme (3.1) with or without the AP correction (3.23) is compared to the solution obtained by a 1D scheme with 1000 points and the DLP scheme on the limit equation (1.10). Both 2D schemes compute the solution on the same coarse mesh composed of 1.5×10^3 cells. The results at time $t_f = 10^{-4}$ are presented in the Figure 14 with a section at $y = 0.5$.

As it can be seen the HLL-DLP scheme with the AP correction is very close to the solution obtained with the diffusive limit, contrary to the same scheme without the AP correction, even on a coarse mesh. The small shift between the 1D and 2D solutions is only due to the initialisation on the coarse mesh. This test case does not need any TP flux correction and the tests need less than 1% of the CPU time.

3.3.2. Convergence to the diffusive limit

In order to have a more quantitative evaluation of the AP property a study of convergence towards the diffusive limit is made. For this study four schemes are used:

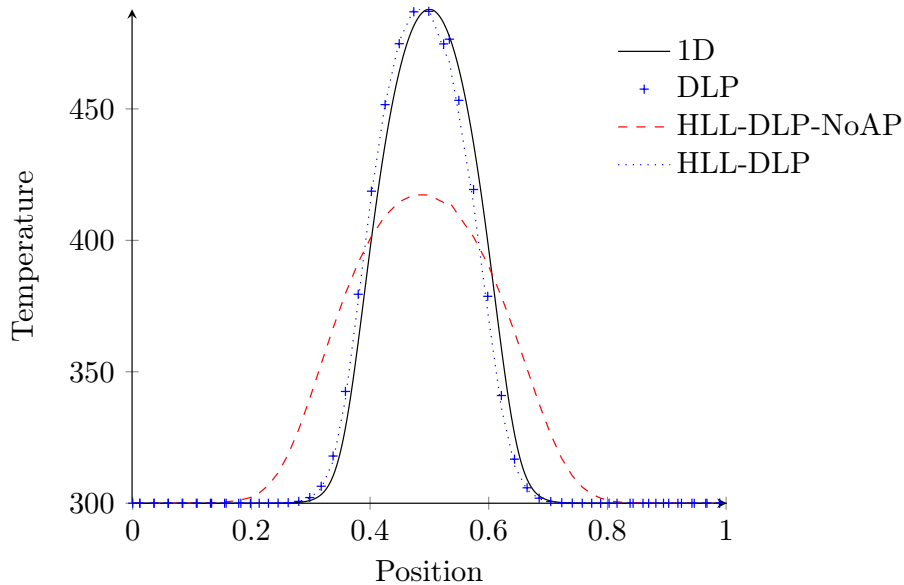


Figure 14: Temperature computed, solid line: parabolic 1D solution; plus marks: DLP solution; dotted line: HLL-DLP solution with AP correction; dashed line: HLL-DLP solution without AP correction

- (S1) the HLL-DLP (3.1) with the AP correction (3.23),
- (S2) the same scheme with the AP correction set to zero ($\bar{\sigma}^m = 0$),
- (S3) the TP flux scheme (2.10) with the source term introduced with the α coefficients,
- (S4) and the TP flux scheme with a centered discretization of the source term.

The M_1 model is used with an initial condition based on a 2D Gaussian in temperature, with the same parameters as in the previous test case:

$$\begin{cases} T_0(x, y) &= 300 \exp\left(-\frac{(x-0.5)^2 + (y-0.5)^2}{2 \times 0.05^2}\right) + 300 \\ E_0(x, y) &= aT_0(x, y)^4 \\ \mathbf{F}_{R,0}(x, y) &= 0 \end{cases} .$$

The computational domain is the unit square $[0; 1]^2$ meshed with 10816 triangles for a space step of $\Delta x \simeq 1.6 \cdot 10^{-3}$ and Neumann boundary conditions are imposed. The L^2 relative errors regarding to the solution obtained with the DLP scheme (2.11) on the limit equation and on the same mesh are presented for different γt in Table 4.

In this table one can see the behaviour of the schemes regarding to the evolution of γt . Indeed, for $\gamma t \Delta x \ll 1$ all the schemes give the same kind of

$\sigma^a, \sigma^e, \sigma^f$	1	5	25	125	625	3125
t	$1/c$	$2/c$	$4/c$	$8/c$	$16/c$	$32/c$
$\gamma t = c\sigma^m t$	1	10^1	10^2	10^3	10^4	10^5
Scheme	L^2 -errors					
(S1)	2.70E-2	1.47E-2	4.63E-3	8.50E-4	2.71E-4	1.12E-4
(S2)	2.70E-2	1.46E-2	3.75E-3	2.86E-3	4.44E-3	3.27E-3
(S3)	2.70E-2	1.46E-2	3.81E-3	2.63E-3	4.05E-3	2.94E-3
(S4)	2.71E-2	1.57E-2	7.58E-3	3.52E-3	1.42E-2	1.92E-2

Table 4: Convergence to the diffusion equation regarding to γt

errors. On the other hand, for $\gamma t \Delta x \gg 1$ the errors of the three schemes which are not AP (S2), (S3) and (S4) do not converge when γt increases and only the AP scheme (S1) provides a decreasing error.

Let us underline that for all the computations with the HLL-DLP scheme, the TP flux correction is never activated and the CPU cost for the tests is inferior to 1%.

3.3.3. Discontinued test case

The next case illustrates the asymptotic behaviour of the HLL-DLP scheme on an unstructured mesh with privileged directions (a triangle is drawn in the center of the mesh, see Figure 15). The isentropic Euler model described by (1.5) is used for this test case.

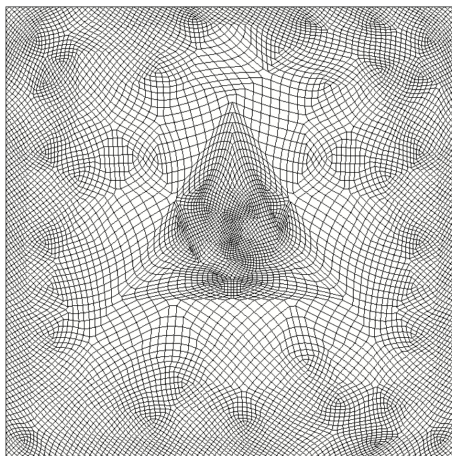


Figure 15: Unstructured mesh with privileged directions

This test case is initialised with $\rho_0 = 1$ inside a circle of radius 0.1 in the center of the domain, and $\rho_0 = 0.1$ elsewhere. Besides, the initial speed is set to zero. The friction coefficient is set to $\kappa = 2000$ and the final time is $t_f = 10$ in order to be close of the diffusive regime.

The solution obtained with the HLL-DLP scheme is compared with three others schemes on a coarse mesh of 9.4×10^3 cells: the DLP scheme on the diffusive equation (1.7), the HLL-DLP scheme without the asymptotic correction (3.19) ($\bar{\kappa} = 0$) and the TP flux scheme. The results are presented in Figure 16. As it can be seen the two not-AP schemes differ totally from the reference

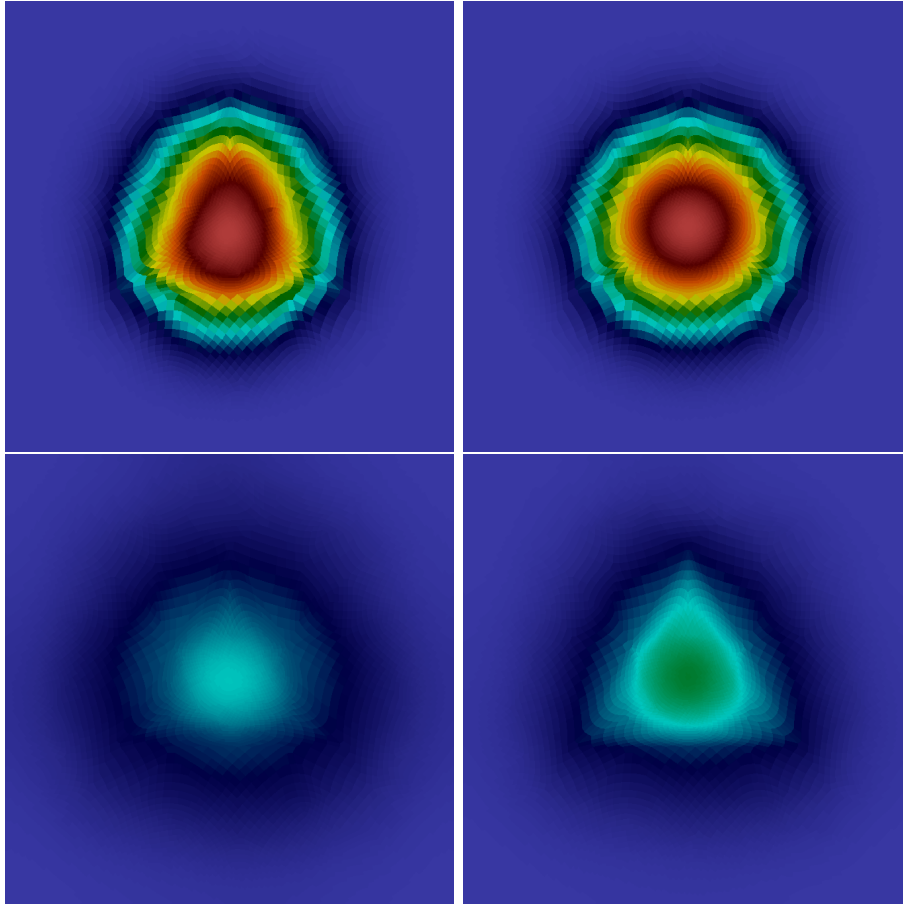


Figure 16: Density results for the circle test case with four schemes (from top to bottom and left to right): the HLL-DLP scheme, the DLP scheme on the diffusion equation, the HLL-DLP scheme without asymptotic correction and the TP scheme

solution (the DLP scheme) as the diffusion is way too large. Moreover, as the diffusion of the TP flux occurs in the direction of the mesh, it significantly diffuses anisotropically. The solution computed with the HLL-DLP scheme is close to the reference solution, even if there is some influence of the mesh: the initial condition is discontinuous, the speed of convergence to the parabolic equation is hence slower than in the continuous case (see [28]). As in the pseudo-1D test case with a Gaussian, this test case does not need the TP flux correction

and the tests for a possible activation of the correction cost less than 1% of the CPU time.

3.3.4. Test case with a space probe

This last test case simply models the entry of a space probe from the ESA: the MSRO (Mars Sample Return Orbiter). The mesh is presented in Figure 17 and the surfaces of the probe are considered as walls. The computational domain is a rectangle $[-6; 8] \times [-5; 5]$, in order to capture most of the phenomenon.

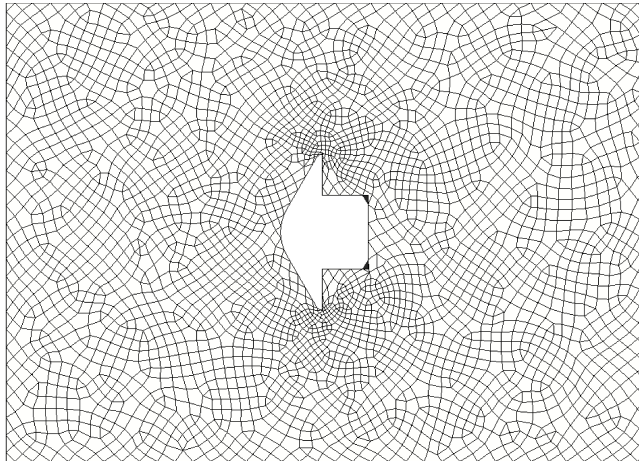


Figure 17: Unstructured mesh around a space probe

A first computation is done with the Euler model, the initial state is $\rho_0 = 1.57005 \times 10^{-5}$, $p_0 = 8.86280 \times 10^{-1}$ without any speed. The left boundary is a Dirichlet condition with \mathbf{u}_0 varying from $\mathbf{u} = (10^3, 0)^T$ to $\mathbf{u} = (10^4, 0)^T$ during 0.05 s, with the same density ρ_0 , and pressure p_0 .

Then, the density and the temperature are extracted from the stationary solution computed at time $t_f = 1$ (see Figure 18), to initialise the M_1 model, with $T_0 = T_{\text{Euler}}$, $E_0 = aT_{\text{Euler}}^4$, and $\mathbf{F}_{R,0} = 0$. The different opacities ($\sigma^a, \sigma^e, \sigma^f$) of the M_1 model follow a non-linear law: $\sigma(T) = \left(\frac{T}{10000}\right)^3 \sigma_0$, with $\sigma_0 = 1500$. The results at time $t_f = 10^{-6}$ are presented in Figure 19.

Even though a realistic computation would involve a full coupling, chemistry and diffusive terms, this simplified example emphasize the fact that in such application, there are zones where the source term is neglectable, zones where the convergence towards the diffusion regime is very fast and in-between regimes. Moreover, these zones depend non-linearly on the time, and can not be predicted. In such a context, a numerical scheme which preserves the asymptotics and the set of admissible states \mathcal{A} is mandatory. The preservation of \mathcal{A} is made thanks to the TP flux correction. For the hyperbolic run, with the ideal gases Euler model, the TP flux correction is needed for almost all the time iterations on less than 1% of the cells with a cost inferior to 2%. Whereas, the run with

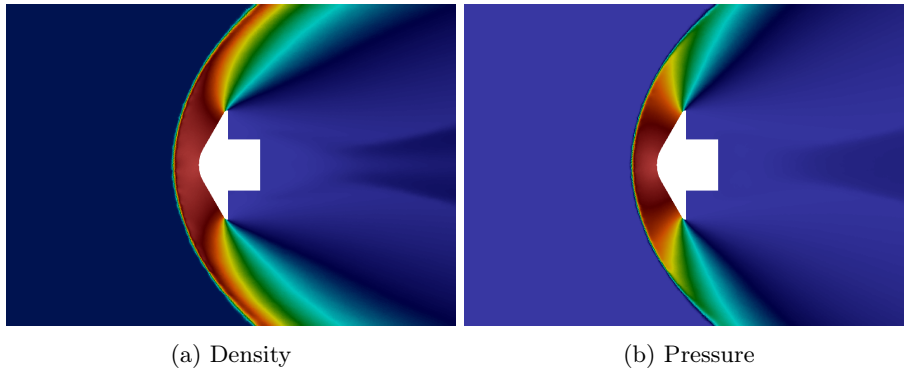


Figure 18: Density and pressure around a space probe computed with the Euler model

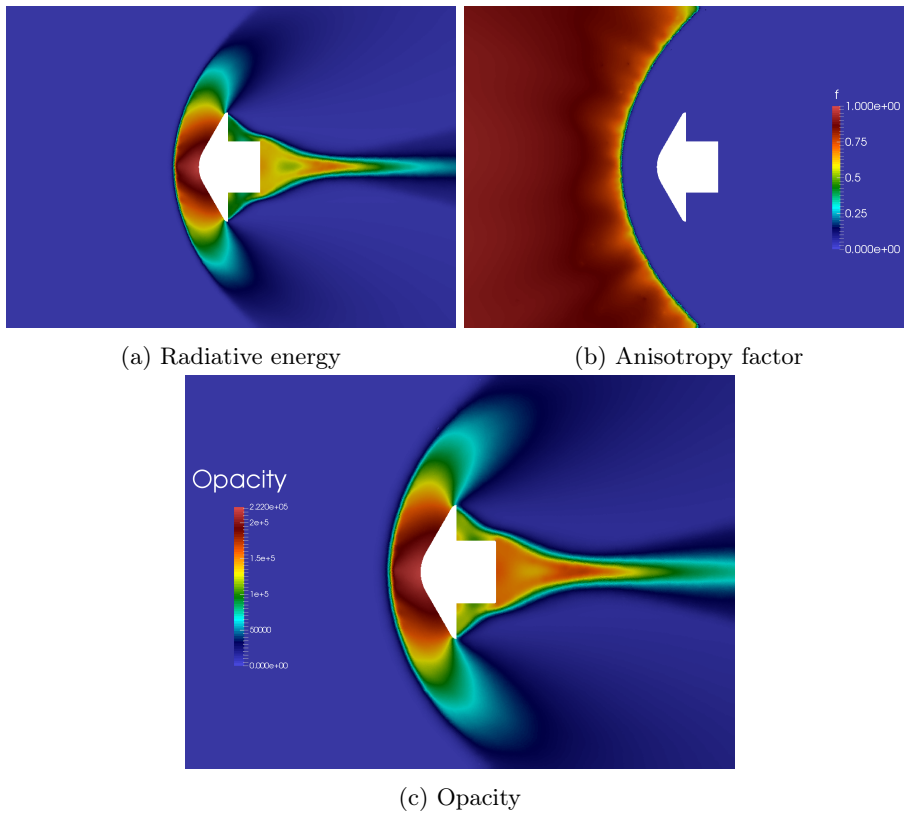


Figure 19: Radiative energy, anisotropy factor and opacity around a space probe computed with the M_1 model

the M_1 model with source term only needs the correction for 5% of the time iterations and the correction is only applied on less than 1% of the cells for a

cost lower to 1%.

Conclusion, extensions

In this work, an admissibility and AP scheme for system of conservation laws of type (1.1) on any unstructured mesh is developed, using the DLP scheme [20] as a limit scheme. The introduction of the source term is done using the technique developed in [7], and the preservation of the set of admissible states \mathcal{A} is guaranteed thanks to an a posteriori correction in the spirit of the MOOD method [17]. This a posteriori correction uses a physical admissibility detector that can be changed to an entropic criterion such as in [3]. The development of a high-order scheme based on the HLL-DLP scheme will be possible for instance using the MOOD method and SSP Runge-Kutta schemes [27] (or the schemes used in [8]). The extension to systems of conservations laws which degenerate into non-linear diffusion equation (e.g. Shallow water with Manning-type friction [22]), or into more complicated system of diffusion equation (for instance the limit of the Euler for ideal gases coupled with the M_1 [5]) has to be developed by extending the DLP scheme in this context.

Acknowledgments

The authors are thankful to G. Moebs for the precious help with the optimization and the improvements in the code.

The authors were funded by the ANR project ACHYLLES (grant number [ANR-14-CE25-0001](#)).

References

- [1] D. Aregba-Driollet, M. Briani, and R. Natalini. Time asymptotic high order schemes for dissipative BGK hyperbolic systems. *Numerische Mathematik*, pages 1–33, 2015.
- [2] C. Berthon, P. Charrier, and B. Dubroca. An HLLC scheme to solve the M_1 model of radiative transfer in two space dimensions. *J. Sci. Comput.*, 31(3):347–389, 2007.
- [3] C. Berthon and V. Desveaux. An entropy preserving MOOD scheme for the Euler equations. *Int. J. Finite Vol.*, 11:39, 2014.
- [4] C. Berthon, J. Dubois, B. Dubroca, T.-H. Nguyen-Bui, and R. Turpault. A free streaming contact preserving scheme for the M_1 model. *Adv. Appl. Math. Mech.*, 2(3):259–285, 2010.
- [5] C. Berthon, P. G. LeFloch, and R. Turpault. Late-time/stiff-relaxation asymptotic-preserving approximations of hyperbolic equations. *Math. Comp.*, 82(282):831–860, 2013.

- [6] C. Berthon, G. Moebis, and R. Turpault. An asymptotic-preserving scheme for systems of conservation laws with source terms on 2D unstructured meshes. In *Finite volumes for complex applications. VII. Methods and theoretical aspects*, volume 77 of *Springer Proc. Math. Stat.*, pages 107–115. Springer, Cham, 2014.
- [7] C. Berthon and R. Turpault. Asymptotic preserving HLL schemes. *Numer. Methods Partial Differential Equations*, 27(6):1396–1422, 2011.
- [8] S. Boscarino, P. G. LeFloch, and G. Russo. High-order asymptotic-preserving methods for fully nonlinear relaxation problems. *SIAM J. Sci. Comput.*, 36(2):A377–A395, 2014.
- [9] F. Bouchut, H. Ounaissa, and B. Perthame. Upwinding of the source term at interfaces for euler equations with high friction. *Comput. Math. Appl.*, 53(3-4):361–375, 2007.
- [10] J. Breil and P.-H. Maire. A cell-centered diffusion scheme on two-dimensional unstructured meshes. *J. Comput. Phys.*, 224(2):785–823, 2007.
- [11] C. Buet and S. Cordier. An asymptotic preserving scheme for hydrodynamics radiative transfer models: numerics for radiative transfer. *Numer. Math.*, 108(2):199–221, 2007.
- [12] C. Buet and B. Després. Asymptotic preserving and positive schemes for radiation hydrodynamics. *J. Comput. Phys.*, 215(2):717–740, 2006.
- [13] C. Buet, B. Després, and E. Franck. Design of asymptotic preserving finite volume schemes for the hyperbolic heat equation on unstructured meshes. *Numer. Math.*, 122(2):227–278, 2012.
- [14] C. Buet, B. Després, and E. Franck. Asymptotic preserving schemes on distorted meshes for Friedrichs systems with stiff relaxation: application to angular models in linear transport. *J. Sci. Comput.*, 62(2):371–398, 2015.
- [15] C. Cancès, M. Cathala, and C. Le Potier. Monotone corrections for generic cell-centered finite volume approximations of anisotropic diffusion equations. *Numer. Math.*, 125(3):387–417, 2013.
- [16] C. Chalons, F. Coquel, E. Godlewski, P.-A. Raviart, and N. Seguin. Godunov-type schemes for hyperbolic systems with parameter-dependent source. The case of Euler system with friction. *Math. Models Methods Appl. Sci.*, 20(11):2109–2166, 2010.
- [17] S. Clain, S. Diot, and R. Loubère. A high-order finite volume method for systems of conservation laws—Multi-dimensional Optimal Order Detection (MOOD). *J. Comput. Phys.*, 230(10):4028–4050, 2011.
- [18] Y. Coudière, J.-P. Vila, and P. Villedieu. Convergence rate of a finite volume scheme for a two-dimensional convection-diffusion problem. *M2AN Math. Model. Numer. Anal.*, 33(3):493–516, 1999.

- [19] G. Dahlquist. A special stability problem for linear multistep methods. *Nordisk Tidskr. Informations-Behandling*, 3:27–43, 1963.
- [20] J. Droniou and C. Le Potier. Construction and convergence study of schemes preserving the elliptic local maximum principle. *SIAM J. Numer. Anal.*, 49(2):459–490, 2011.
- [21] B. Dubroca and J. Feugeas. Theoretical and numerical study of a moment closure hierarchy for the radiative transfer equation. *C. R. Acad. Sci. Paris Sér. I Math.*, 329(10):915–920, 1999.
- [22] A. Duran, F. Marche, R. Turpault, and C. Berthon. Asymptotic preserving scheme for the shallow water equations with source terms on unstructured meshes. *J. Comput. Phys.*, 287:184–206, 2015.
- [23] R. Eymard, T. Gallouët, and R. Herbin. Finite volume methods. In *Handbook of numerical analysis, Vol. VII*, Handb. Numer. Anal., VII, pages 713–1020. North-Holland, Amsterdam, 2000.
- [24] M. S. Floater. Mean value coordinates. *Comput. Aided Geom. Design*, 20(1):19–27, 2003.
- [25] E. Franck. *Design and numerical analysis of asymptotic preserving schemes on unstructured meshes. Application to the linear transport and Friedrichs systems*. PhD thesis, Université Pierre et Marie Curie - Paris VI, October 2012.
- [26] L. Gosse and G. Toscani. An asymptotic-preserving well-balanced scheme for the hyperbolic heat equations. *C. R. Math. Acad. Sci. Paris*, 334(4):337–342, 2002.
- [27] S. Gottlieb, C.-W. Shu, and E. Tadmor. Strong stability-preserving high-order time discretization methods. *SIAM Rev.*, 43(1):89–112, 2001.
- [28] B. Hanouzet and R. Natalini. Global existence of smooth solutions for partially dissipative hyperbolic systems with a convex entropy. *Arch. Ration. Mech. Anal.*, 169(2):89–117, 2003.
- [29] A. Harten, P. D. Lax, and B. van Leer. On upstream differencing and Godunov-type schemes for hyperbolic conservation laws. *SIAM Rev.*, 25(1):35–61, 1983.
- [30] S. Jin and C. D. Levermore. Numerical schemes for hyperbolic conservation laws with stiff relaxation terms. *J. Comput. Phys.*, 126(2):449–467, 1996.
- [31] A. Kurganov and E. Tadmor. Solution of two-dimensional Riemann problems for gas dynamics without Riemann problem solvers. *Numer. Methods Partial Differential Equations*, 18(5):584–608, 2002.

- [32] C. Le Potier. Correction non linéaire et principe du maximum pour la discrétisation d'opérateurs de diffusion avec des schémas volumes finis centrés sur les mailles. *C. R. Math. Acad. Sci. Paris*, 348(11-12):691–695, 2010.
- [33] C. Le Potier. Correction non linéaire d'ordre 2 et principe du maximum pour la discrétisation d'opérateurs de diffusion. *C. R. Math. Acad. Sci. Paris*, 352(11):947–952, 2014.
- [34] C. D. Levermore. Moment closure hierarchies for kinetic theories. *J. Statist. Phys.*, 83(5-6):1021–1065, 1996.
- [35] P. Marcati and A. Milani. The one-dimensional Darcy's law as the limit of a compressible Euler flow. *J. Differential Equations*, 84(1):129–147, 1990.
- [36] D. Mihalas and B. Weibel-Mihalas. *Foundations of Radiation Hydrodynamics*. Dover Books on Physics. Dover, 1999.
- [37] B. Perthame and C.-W. Shu. On positivity preserving finite volume schemes for Euler equations. *Numer. Math.*, 73(1):119–130, 1996.
- [38] G.C. Pomraning. *The equations of radiation hydrodynamics*. International series of monographs in natural philosophy. Pergamon Press, 1973.
- [39] V. V. Rusanov. The calculation of the interaction of non-stationary shock waves with barriers. *Ž. Vyčisl. Mat. i Mat. Fiz.*, 1:267–279, 1961.
- [40] C. Sarazin Desbois. *Numerical methods for hyperbolic systems with source term issuing from complex physic for radiation*. PhD thesis, Université de Nantes, March 2013.
- [41] C. W. Schulz-Rinne. Classification of the Riemann problem for two-dimensional gas dynamics. *SIAM J. Math. Anal.*, 24(1):76–88, 1993.
- [42] E. F. Toro. *Riemann solvers and numerical methods for fluid dynamics*. Springer-Verlag, Berlin, third edition, 2009. A practical introduction.
- [43] E. F. Toro, M. Spruce, and W. Speares. Restoration of the contact surface in the HLL-Riemann solver. *Shock Waves*, 4(1):25–34, 1994.
- [44] P. Woodward and P. Colella. The numerical simulation of two-dimensional fluid flow with strong shocks. *J. Comput. Phys.*, 54(1):115–173, 1984.
- [45] T. Zhang and Y. X. Zheng. Conjecture on the structure of solutions of the Riemann problem for two-dimensional gas dynamics systems. *SIAM J. Math. Anal.*, 21(3):593–630, 1990.

D. Asymptotic preserving modification for the HLL flux

The use of the HLL flux for the base flux implies some modifications in the definition of α_{KJ} and then in the asymptotic correction $\bar{\gamma}_{K,i}^J$

With b_{KJ}^+ and b_{KJ}^- the wave speeds the HLL flux [29] reads:

$$\mathcal{F}_{KJ} \cdot \boldsymbol{\eta}_{KJ} = \frac{-b_{KJ}^-}{b_{KJ}^- - b_{KJ}^+} \mathbf{F}(\mathbf{U}_J^n) + \frac{b_{KJ}^+}{b_{KJ}^- - b_{KJ}^+} \mathbf{F}(\mathbf{U}_K^n) + \frac{b_{KJ}^- b_{KJ}^+}{b_{KJ}^- - b_{KJ}^+} (\mathbf{U}_J^n - \mathbf{U}_K^n) \quad (\text{D.1})$$

Then the based flux for the complete system (1.1) is:

$$\begin{aligned} \bar{\mathcal{F}}_{KJ} \cdot \boldsymbol{\eta}_{KJ} &= \alpha_{KJ} \mathcal{F}_{KJ} \cdot \boldsymbol{\eta}_{KJ} - (\alpha_{KJ} - \alpha_{KK}) \mathbf{F}(\mathbf{U}_K^n) \cdot \boldsymbol{\eta}_{KJ} \\ &\quad - (1 - \alpha_{KJ}) \frac{b_{KJ}^+ - b_{KJ}^-}{2} (\mathbf{R}(\mathbf{U}_K^n) - \mathbf{U}_K^n), \end{aligned} \quad (\text{D.2})$$

where $\mathcal{F}_{KJ} \cdot \boldsymbol{\eta}_{KJ}$ is the HLL flux previously defined the α coefficients are defined as following:

$$\begin{cases} (\alpha_{KJ})^j &= \alpha_{KJ}^j = \frac{(b_{KJ}^+ - b_{KJ}^-)}{(b_{KJ}^+ - b_{KJ}^-) + 2\gamma_K \delta_{KJ}^j} \in [0; 1] \\ \alpha_{KK} &= \frac{b_{KK}^- - b_{KK}^+}{(b_{KK}^- - b_{KK}^+) + 2\gamma_K \delta_{KK}^K}, \text{ with } \delta_{KK}^K = \frac{|K|}{p_K}. \end{cases} \quad (\text{D.3})$$

For the isentropic Euler model the limit scheme is now:

$$\rho_K^{n+1} = \rho_K^n + \sum_{i \in \mathcal{E}_K} \frac{\Delta t}{|K|} |e_i| \sum_{J \in \mathcal{S}_{K,i}} \nu_{K,i}^{J,\rho} \frac{-b_{KJ}^+ b_{KJ}^-}{2(\kappa_K + \bar{\kappa}_{K,i}^J) \delta_{KJ}^\rho} (\rho_J - \rho_K). \quad (\text{D.4})$$

And therefore the correction $\bar{\kappa}$ needs to be chosen such that:

$$\bar{\kappa}_{K,i}^J = \kappa_K \left(\frac{\nu_{K,i}^{J,\rho} (-b_{KJ}^+ b_{KJ}^-)}{2\bar{\nu}_{K,i}^J \delta_{KJ}^\rho} \frac{\rho_J - \rho_K}{p_J - p_K} - 1 \right), \quad (\text{D.5})$$

in order to have the following limit scheme:

$$\rho_K^{n+1} = \rho_K^n + \sum_{i \in \mathcal{E}_K} \frac{\Delta t}{|K|} |e_i| \sum_{J \in \mathcal{S}_{K,i}} \frac{\bar{\nu}_{K,i}^J}{\kappa_K} (p_J - p_K), \quad (\text{3.20})$$

Let us notice that those results fall back to the one described with the Rusanov flux described previously by setting $b^+ = -b^-$.

And for the M_1 model:

$$\begin{aligned} (\rho C_v T + aT^4)_K^{n+1} &= (\rho C_v T + aT^4)_K^n \\ &\quad + \sum_{i \in \mathcal{E}_K} \frac{\Delta t}{|K|} |e_i| \sum_{J \in \mathcal{S}_{K,i}} \nu_{K,i}^{J,E} \frac{-b_{KJ}^- b_{KJ}^+}{2c((\sigma^m)_K + (\bar{\sigma}^m)_{K,i}^J) \delta_{KJ}^E} ((aT^4)_J - (aT^4)_K), \end{aligned} \quad (\text{D.6})$$

which leads to this AP correction:

$$(\bar{\sigma}^m)^J_{K,i} = 3(\sigma^f)_K \frac{-b^-_{KJ} b^+_{KJ} \nu_{K,i}^{J,E}}{2c^2 \bar{\nu}^J_{K,i} \delta^E_{KJ}} - (\sigma^m)_K. \quad (\text{D.7})$$

We could also use an HLLC scheme (see [43, 42] for Euler and [2, 4] for the M_1 model), this will also modify the values of α and $\bar{\gamma}$.